A comparative study of electrical interfaces for tunable piezoelectric vibration energy harvesting

Adrien Morel, Alexis Brenes, David Gibus, Elie Lefeuvre, Pierre Gasnier, Gaël Pillonnet, Adrien Badel

A Comparative Study of Electrical Interfaces for Tunable Piezoelectric Vibration Energy Harvesting

Adrien Morel[1], Alexis Brenes[2], David Gibus[1], Elie Lefeuvre[2], Pierre Gasnier[3], Gaël Pillonnet[3], Adrien Badel[1]

[1] Université Savoie Mont-Blanc, SYMME, F-74940 Annecy, France
[2] Centre for Nanoscience and Nanotechnology, Univ. Paris Sud–CNRS, Université Paris-Saclay, France
[3] Université Grenoble Alpes, CEA, LETI, MINATEC, F-38000 Grenoble, France

E-mail: adrien.morel@univ-smb.fr
Received xxxxxx
Accepted for publication xxxxxx
Published xxxxxx

Abstract

The present work deals with tunable electrical interfaces able to enhance both the harvested power and bandwidth of piezoelectric vibration energy harvesters. The aim of this paper is to propose a general, normalized, and unified performance evaluation (with respect to the harvested power and bandwidth) of the various electrical strategies that can tune the harvester's frequency response. By mean of a thorough analysis, we demonstrate how such interfaces influence the electromechanical generator response through an electrically-induced damping and an electrically-induced stiffness. The choice of the strategy determines these two electrical quantities, and thus the achievable frequency response of the system. Thereafter, we introduce a collection of graphical and analytical tools to compare and analyze single- and multi-tuning electrical strategies, including a qualitative performance evaluation of existing strategies. Finally, we establish a unified comparison of single- and multiple-tuning strategies which is supported by the definition and evaluation of a new optimization criterion. This comparison reveals which strategy performs best depending on the electromechanical coupling of the piezoelectric harvester and on the losses in the electrical interface. Furthermore, it quantifies the power and bandwidth gain brought by single- and multi-tuning strategies. Such quantitative criterion provides guidance for the choice of a harvesting strategy in any specific applicative case.

Keywords: Piezoelectric vibration energy harvester, Electrical strategies, Adaptive interfaces, Frequency tuning, Comparison.

1. Introduction

Piezoelectric vibration energy harvesters (PEH) convert energy from ambient vibrations into storable electrical energy that can be used to power sensors. Electrical interfaces for PEH come as a variety of strategies that have been attracting research interests for many years (for reviews, see e.g. [1] and [2]). The initial aim of PEH electrical interfaces is to extract the energy from PEH, rectify the piezoelectric voltage, and eventually store the collected energy [3]. In real environments, the vibration amplitude and frequency might vary with time. In order to optimize the collected energy in such environments, researchers proposed to additionally use electrical interfaces to adjust the PEH resonance frequency to make it as close as possible to the vibration frequency [4] [5]. Such tunable electrical interfaces enable the design of adaptive vibration energy harvesters to compensate for aging effects or environmental changes. However, the tradeoff between several design criteria such as bandwidth, extracted power, and/or power conversion efficiency—all dependent on the transducer characteristics—makes a general comparison difficult. Here, we introduce graphical and analytical tools to analyze existing electrical strategies. Based on these tools, we propose a unified evaluation and comparison of PEH electrical interfaces. In order to maximize the harvested power from a PEH, two parameters must be considered: the harvester resonance frequency, and the damping induced by the electrical interface [6]. Because of the relatively weak electromechanical coupling of most PEH in 1995-2010, the effect of the electrical interface on the resonance frequency was initially too small to be useful [7]. This explains why the first interface circuits developed in the literature aimed at maximizing the electrical damping without considering the resonance frequency. This was the case for the standard energy harvesting (SEH) interface [8], the Parallel and Series Synchronized Switch Harvesting on Inductance (P-SSHI and S-SSHI) [9], and the Synchronous Electrical Charge Extraction (SECE) [10]. All these circuits exhibit a single tuning parameter (or even no tuning parameter

in the case of the SECE) that must be tuned to maximize the extracted energy. Many improvements of the aforementioned interfaces have flourished in the literature, to further increase the electrical damping and maximize the extracted power for weakly coupled harvesters. For instance, the Synchronized Switch Harvesting on Capacitors (SSHC) is a compact version of the SSHI that uses capacitors to implement the voltage inversion [11]. The Tunable SECE [12] and Synchronous Electric Charge Partial Extraction (SECPE) [13] are two strategies derived from the SECE that exhibit a single tuning parameter that is used to maximize the electrical damping. Since the electromechanical coupling of piezoelectric vibration energy harvesters is increasingly strong as a consequence of material improvement and dimensional optimizations [14][15], some researchers recently proposed new strategies that exploit this coupling in order to tune PEH resonance frequency. For instance, single-tuning strategies such as the Phase-shifted SECE (PSSECE) [16], the shorted SECE (SSECE) [17] and the N-SECE [6] allow simultaneous control over both the electrical damping and the resonance frequency of the system. However, to control the PEH resonance frequency and electrical damping independently, a second tuning parameter is required [1]. Some recent strategies such as the Frequency Tuning SECE (FTSECE) [18], the Short-Circuit SECE (SCSECE) [19], the Phase-shifted SSHI (PS-SSHI) [20][21], and the Tunable Hybrid SSHI (TH-SSHI) [22] exhibit two tuning parameters, making them particularly efficient when associated with strongly coupled PEH. Therefore, many electrical strategies have already been designed for harvesting energy from both weak coupling and strong coupling harvesters. However, there is still a need to unify the two views, and determine a quantitative approach that defines the weaknesses and strengths of each particular electrical strategy depending on the PEH coupling. Furthermore, determining which strategy is the best in each case remains an open question that needs to be answered by a systemic approach.

In this paper, we propose a thorough comparison of tunable electrical interfaces for piezoelectric vibration energy harvesting. The second and third sections recall the dynamics of linear piezoelectric harvesters connected to electrical interfaces exhibiting tuning parameters. We gather the electrical influences on the harvester's frequency response under two dimensionless terms that correspond to an electrically-induced stiffness and an electrically-induced damping. Based on these well-established models, the fourth section introduces the formalism and tools that are applied in the fifth section to analyze and evaluate some well-known tunable strategies found in the literature. Finally, based on a new quantitative criterion (defined as the integral of the harvested power envelope, normalized by the integral of a reference envelope), the sixth section of this paper presents a unified comparison of single- and multi-parameter tuning interfaces.

2. Electromechanical modelling of linear PEH

2.1 Dynamics of the electromechanical harvester

A piezoelectric harvester is traditionally made of piezoelectric material layers bonded to a mechanical resonator. In this paper, we focus on single-degree-of-freedom (SDOF) PEH.

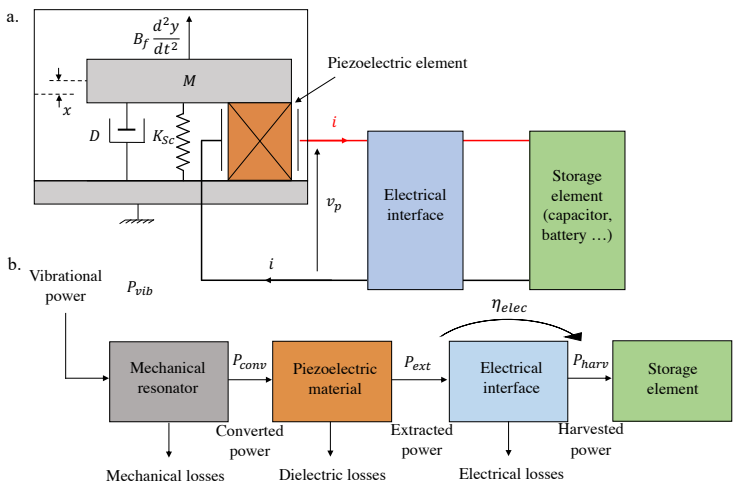

Figure 1. a. Single-degree-of-freedom piezoelectric energy harvesting system model, and b. its associated energy model. The electrical efficiency is defined in [23].

We assume that the mechanical behavior of the transducer is linear (i.e., linear mechanical damping and linear mechanical stiffness). As detailed in [24], an SDOF linear PEH can be modelled as an inertial mass M attached to a mechanical damper D and a spring of stiffness K_{sc}, as shown in Fig.1.a. The piezoelectric material under strain generates a quantity of electrical charges proportional to the mechanical displacement x of the mass. These charges are either stored in the piezoelectric material capacitance C_p or collected into an electrical interface drawing an electrical current i. Owing to the converse piezoelectric effect, the piezoelectric element exerts a force (αv_p) on the inertial mass, which is proportional to the voltage v_p across the piezoelectric material. In this paper, we assume that:

i) The external displacement $y(t)$—and the associated acceleration $\gamma(t)$—is sinusoidal and we can write $\frac{d^2y(t)}{dt^2} = \gamma_m \sin(\omega t)$ with γ_m being the acceleration magnitude and ω its pulsation.

ii) The amplitude of the vibration remains relatively small, and does not induce any significant nonlinear effect in the mechanical resonator or inside the piezoelectric material.

iii) The harvester exhibits a relatively large mechanical quality factor $(Q_m > 10)$. This assumption is valid for most harvesters in the literature ([6], [14], [20]) that operate at low-frequency and in low-power applications (typically smaller than 1kHz and 10mW).

iv) The influence of the higher mechanical modes is considered negligible.

v) The dielectric losses are negligible, compared to other power losses. This last assumption is reasonable for piezoelectric ceramics that usually exhibit high dielectric permittivity, as long as the electric field in the piezoelectric material remains relatively low [25], [26].

The aforementioned assumptions are generally valid for ceramic-based PEH [4], but can also be extended to polymers and composites as long as the linear assumption remains reasonable. They lead to (1) which describes the dynamics of the system.

$$\begin{cases} M\frac{d^2x(t)}{dt^2} + D\frac{dx(t)}{dt} + K_{sc}\,x(t) + \alpha\, v_p(t) = -B_f\frac{d^2y(t)}{dt^2} \\ i(t) = \alpha\frac{dx(t)}{dt} - C_p\frac{dv_p(t)}{dt} \end{cases} \quad (1)$$

Where α represents the force factor of the harvester, y the external displacement applied on the whole electromechanical system, and B_f the forcing term considering the input acceleration. (1) can be reformulated with dimensionless variables (defined in Table 1) in order to obtain (2) [1].

$$\begin{cases} \ddot{X}(\theta) + \dot{X}(\theta)/Q_m + X(\theta) + U(\theta) = -\ddot{Y} \\ I(\theta) = k_m^2 \dot{X}(\theta) - \dot{U}(\theta) \end{cases} \quad (2)$$

Where $Q_m = \sqrt{K_{sc}M}/D$ is the mechanical quality factor of the resonator and $k_m^2 = \alpha^2/(K_{sc}C_p)$ is the expedient electromechanical coupling coefficient. The dotted notation refers to the derivative with respect to the angle $\theta = \omega_0 t$, and $\omega_0 = \sqrt{K_{sc}/M}$ is the short-circuit resonance pulsation of the harvester. As long as the assumptions (i-v) remain valid, the system (2) accurately models the dynamics of SDOF linear piezoelectric energy harvesters [1]. This model allows to make reliable predictions of the harvested power and has been experimentally validated with various piezoelectric energy harvesters and interface circuits, as reported in the literature (e.g., [4], [6], [16]).

Table 1. Physical variables and their normalized expressions

Variable	Quantity (unit)	Normalized variable
ω	Vibration pulsation (rad.s^{-1})	$\Omega = \omega/\omega_0$
y	External displacement (m)	$Y = B_f y \omega_0^2/(M\gamma_m)$
x	Displacement of the mass M (m)	$X = x\omega_0^2/\gamma_m$
i	Piezoelectric current (A)	$I = \alpha i/(C_p M \omega_0 \gamma_m)$
v_p	Piezoelectric voltage (V)	$U = \alpha v_p/(M\gamma_m)$

3. Influences of the electrical interface on the PEH's frequency response

In this section, we derive how the electrical interface impacts the harvester's frequency response.

3.1 Electrically-induced damping and stiffness

In the frequency domain, the transfer function between the first-harmonic U_1 of the piezoelectric voltage and the first-harmonic X_1 of the displacement can be written as (3) [4],

$$\frac{\underline{U_1}}{\underline{X_1}} = k_m^2(\varepsilon_K(\Omega) + j\varepsilon_D(\Omega)) \quad (3)$$

with ε_D and ε_K being two dimensionless variables representing the electrically-induced damping and stiffness. This physically means that the electrically-induced force applied on the resonator (due to the converse piezoelectric effect) has an in-phase term (ε_K) and an out-of-phase term (ε_D) with the mechanical displacement. The in-phase term contributes to an additional stiffness while the out-of-phase term contributes to an additional damping, both being electrically-induced. As a result of the first-harmonic assumption (detailed in Appendix B), all the influences of the electrical interface on the harvester's frequency response can be gathered under these two terms, even if the electrical interface behaves nonlinearly. By combining (22) and (24) of Appendix A with (3), we express the conditions of optimality of ε_D and ε_K that maximize the extracted power as follows:

$$\begin{cases} \varepsilon_{D,opt} = \dfrac{\Omega}{k_m^2 Q_m} \\ \varepsilon_{K,opt} = \dfrac{\Omega^2 - 1}{k_m^2} \end{cases} \quad (4)$$

(4) combined with the first-harmonic assumption (Appendix B) prove that a fine electrical tuning of ε_D and ε_K could lead to extract the power limit P_{lim}—whose expression is recalled in Appendix A—for any linear harvester, and for any vibration frequency. Equation (4) also shows that a stronger electromechanical coupling k_m^2 leads to lower optimal values of ε_D and ε_K.

3.2 Extracted power as a function of ε_D and ε_K

Rewriting the first equation of (2) in the frequency domain, we obtain (5).

$$\underline{X}\left[(1-\Omega^2) + j\frac{\Omega}{Q_m}\right] + \underline{U} = \Omega^2 \underline{Y} \quad (5)$$

Combining (5) with (3) under the first-harmonic assumption (Appendix B), we obtain the expression of $\underline{X}$ in the frequency domain:

$$\underline{X} = \frac{\Omega^2 \underline{Y}}{(1 - \Omega^2 + k_m^2 \varepsilon_K(\Omega)) + j\left(\frac{\Omega}{Q_m} + k_m^2 \varepsilon_D(\Omega)\right)} \quad (6)$$

We can observe from (6) why ε_D and ε_K can be considered as electrical damping and stiffness, respectively. Indeed, any change in ε_K impacts the resonance frequency Ω_{res} of the system as Ω_{res} is the solution of $(1 - \Omega_{res}^2 + k_m^2 \varepsilon_K(\Omega_{res})) = 0$. On the other hand, any change in ε_D modifies the damping of the system. Rewriting the second equation of (2) in the frequency domain, taking its complex conjugate, and multiplying both sides by $U(\theta)$, we obtain the apparent extracted power S_{ext}:

$$S_{ext} = \frac{4P_{lim}k_m^2\Omega}{Q_m}(-j(1-\varepsilon_K) + \varepsilon_D)(\varepsilon_K + j\varepsilon_D)\left|\underline{X}\right|^2 \quad (7)$$

Taking the real part of S_{ext} leads to the expression of the normalized extracted power $P_{nor} = P_{ext}/P_{lim}$.

$$P_{nor} = \frac{4k_m^2\, \varepsilon_D(\Omega)\frac{\Omega}{Q_m}}{\left(1 - \Omega^2 + k_m^2\varepsilon_K(\Omega)\right)^2 + \left(\frac{\Omega}{Q_m} + k_m^2\varepsilon_D(\Omega)\right)^2} \quad (8)$$

$P_{nor} \in [0,1]$ is a measure of how well a harvesting interface is able to extract a power close to the power limit, and depends on the harvester's key parameters, k_m^2 and Q_m. By determining the expressions of ε_D and ε_K of the existing electrical strategies, we can express, from (8), their normalized power vs frequency responses for any linear harvester. If the condition of optimality given by (4) is fulfilled, the normalized extracted power is equal to its upper bound ($P_{ext} = P_{\lim}$):

$$\forall(\Omega, k_m^2) \in (\mathbb{R}^+\backslash\{0\})^2, P_{nor}\left(\varepsilon_{D_{opt}}, \varepsilon_{K_{opt}}\right) = 1 \quad (9)$$

Based on (8), the conditions given by (4) can be understood as the following two propositions:

- The resonance of the electromechanical system should match the vibration frequency [4].
- At resonance, the damping induced by the electrical interface should be equal to the mechanical damping.

4. Tools for the comparison of tunable strategies

In this section, we present the tools required for a unified comparison and analysis of tunable strategies in the literature.

4.1 Toward an electrical control of the PEH's frequency response

Equation (9) given in *Section 3.2* proves that the power limit $P_{\lim}$ can be extracted for any harvester and any vibration frequency as soon as the electrical damping and stiffness are equal to their optimal expressions given by (4). However, these optimal parameters depend on the vibration frequency, meaning that they need to be constantly adjusted as the vibration frequency changes. They also need to be adjusted with the variations of Q_m, ω_0, and k_m^2 which might, for instance, be caused by aging or temperature shifts [27]. In order to make ε_D and ε_K adjustable, we define a set of k parameters $\psi_i \in \mathbb{V}_i$, with $i \in \{1, k\}$ being the parameter index, and $\mathbb{V}_i$ the domain of definition of the i^{th} parameter. These k parameters must be electrically adjustable, and have an impact on the piezoelectric voltage waveform. They can, for instance, correspond to the instant when the energy is extracted from the harvester into the electrical interface [16], the quantity of charges reinjected in the harvester every semi period of vibration [13], or the capacitance of a capacitor placed in parallel with the piezoelectric material [28]. As a result of these adjustable parameters, the electrical damping as well as the electrical stiffness become functions of ψ_i. Obviously, the expressions of these functions, as well as the domains of definition $\mathbb{V}_i$, depend on the choices of the tunable parameters ψ_i. Thus, we label an electrical strategy that introduces at least one tunable parameter ($k \geq 1$) that influences ε_D and/or ε_K as *tunable electrical strategy.*

4.2 Electromechanical Influence Chart (EIC)

A way to visualize the potential performances of a tunable electrical strategy is to plot all possible couples $(\varepsilon_D, \varepsilon_K)$ associated with this strategy. The electromechanical influence of a strategy can be plotted as in Fig.2.a where the x-axis represents ε_D and the y-axis ε_K. The vertical blue-to-purple lines represent the optimal couple $\left(\varepsilon_{D_{opt}}, \varepsilon_{K_{opt}}\right)$ for a harvester exhibiting a given k_m^2 $\left(\forall \Omega \in \mathbb{R}^{+^*}\right)$. These blue-to-purple lines show which region should be reached if one wants to maximize the extracted power for any particular vibration frequency for a given electromechanical coupling. Meanwhile, the green-to-red lines represent the optimal $\left(\varepsilon_{D_{opt}}, \varepsilon_{K_{opt}}\right)$ at a given frequency Ω $\left(\forall k_m^2 \in \mathbb{R}^{+^*}\right)$. The point of intersection of a red-to-green line with a blue-to-purple line represents the unique couple $\left(\varepsilon_{D_{opt}}, \varepsilon_{K_{opt}}\right)$ maximizing the extracted power for a particular association of a vibration frequency and electromechanical coupling. Each electrical interface can consequently be represented in the $(\varepsilon_D, \varepsilon_K)$ plane by a single dot (if this interface does not include any tuning, $k = 0$), a directed smooth curve $\mathcal{C}_{strategy}$ (single-tuning interfaces, $k = 1$) or a surface $\mathcal{S}_{strategy}$ (multi-tuning interfaces, $k \geq 2$).

For instance, the dots (A, B, C) correspond to three couples $(\varepsilon_D, \varepsilon_K)$ maximizing the extracted power for $k_m^2 = 0.070$ and for three vibration frequencies Ω, as detailed in Table 2. The dots (A', B', C') correspond to three other couples $(\varepsilon_D, \varepsilon_K)$ maximizing the extracted power for a weaker coupling, $k_m^2 = 0.015$. Figure 2.b. and 2.c. show the power frequency responses associated with those couples. A comparison between Fig. 2.b. and Fig. 2.c. shows that for an interface able to tune ε_K in a finite range, a stronger coupling leads to an increase of the frequency tuning range, and consequently to a larger harvesting bandwidth. We can verify that the optimal electrical damping decreases as the coupling is increased. Note that the EIC is very similar to the impedance plot previously introduced in [29], except that the focus is on the mechanical side of the PEH instead of the electrical side.

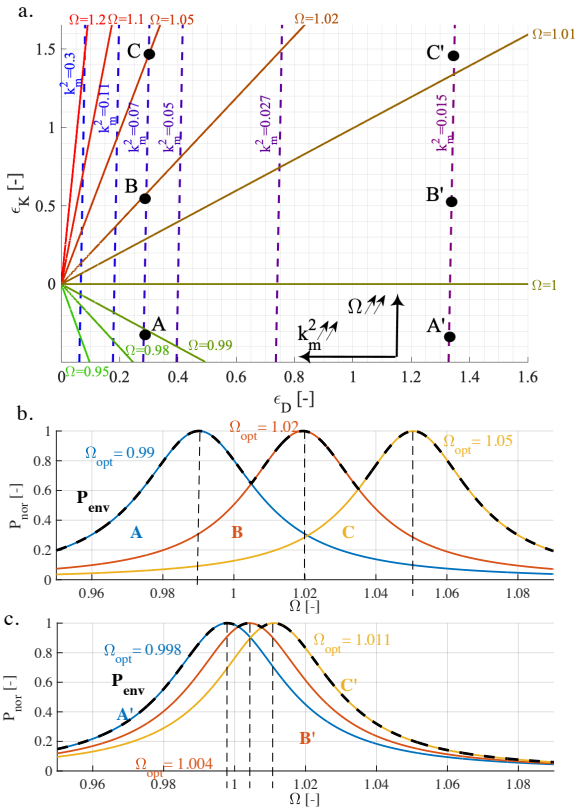

Figure 2. a. EIC showing optimal Ω and k_m^2 in the $(\varepsilon_D, \varepsilon_K)$ plane, b. power frequency responses corresponding to the dots A, B and C (coupling $k_m^2 = 0.07$ $Q_m = 50$) and the obtained power envelope P_{env} c. power frequency responses corresponding to the dots A', B' and C' ($k_m^2 = 0.015, Q_m = 50$), and the obtained power envelope P_{env}.

Table 2. Optimal vibration frequency for the dots on Fig.2

Dot	ε_D	ε_K	k_m^2	Ω_{opt}
(A)	0.28	-0.28	0.070	0.990
(B)	0.28	0.56	0.070	1.020
(C)	0.28	1.48	0.070	1.050
(A')	1.33	-0.28	0.015	0.998
(B')	1.33	0.56	0.015	1.004
(C')	1.33	1.48	0.015	1.010

While the EIC constitutes a useful tool to visualize all the electrical influences linked with a particular strategy, it also has some limitations. The main issue with the EIC is that it only allows an estimation of the extracted power with a particular strategy, and not the net harvested power in a storage element (Fig.1.b.).

4.3 Relations between extracted and harvested powers

In order to take into account the interface losses when they appear to be non-negligible, the electrical efficiency $\eta_{elec} \in [0,1]$ is defined as follows:

$$\eta_{elec} = \frac{P_{harv}}{P_{ext}} = \frac{P_{harv}}{P_{nor}\, P_{lim}} \tag{10}$$

where P_{harv} is the net harvested DC power in a storage element of the electrical interface (i.e., a capacitor or a battery). This

electrical efficiency is strategy- and topology-dependent. Expressions of this electrical efficiency have already been derived for various electrical strategies in [23], and will be used in the next sections of this paper.

4.4 Power envelopes of electrical strategies

Any combination of values taken by the k parameters of a strategy can be associated with a single couple of electrical influence $(\varepsilon_D, \varepsilon_K)$ and with a given harvested power vs frequency response $P_{nor}(\Omega)$ (8). The power-frequency response of the harvester can be adjusted in real-time by tuning ψ_i. Another way to evaluate the performances of a tunable electrical strategy (while taking the electrical efficiency into account) is to compute its power envelope $P_{env}(\Omega)$, defined by (11).

$$\forall i \in \{1,k\}, P_{env}(\Omega) = \max\{\eta_{elec} P_{nor}(\Omega, \psi_i); \psi_i \in \mathbb{V}_i\} \quad (11)$$

The power envelope represents the maximum harvested power of a tunable strategy with a fine optimization of the k tunable parameters at each vibration frequency. This shows the power limit that can be achieved with a particular electrical strategy and is a good indication of its ability to tune the PEH's frequency response. This power envelope has already been used in a few papers studying tunable electrical strategies [6][19][4].

5. Unified analysis of tuning strategies in the literature

In this section, we evaluate the performances of existing tunable strategies by means of the aforementioned graphical tools. In order to organize this section, we classify the existing tunable electrical strategies in two families - Constant Voltage Extraction and Constant Displacement Extraction strategies - with an energy-based classification. This classification proves to be relevant since the choice of tuning parameters and the expression of the electrical efficiency (10) depend on the family (CVE or CDE) of a strategy, as explained in the following sections.

5.1 Proposed classification of tunable strategies

5.1.1 Constant Displacement Extraction Strategies

The proposed classification of electrical strategies relies on energetic considerations, depending on which physical quantity remains unchanged between the start and the end of the energy extraction process. If the energy is extracted from the piezoelectric material within a very short time (compared to the period of mechanical vibration) - resulting in a negligible variation of the mechanical displacement between the start and the end of the energy extraction phase - then the strategy will be classified as a Constant Displacement Extraction (CDE) strategy. A well-known interface that can be classified as a CDE is the SECE. Indeed, as shown in Fig. 3, the energy is extracted from the piezoelectric harvester when the mechanical displacement x is constant and equal to $\pm x_{max}$. Thereafter, the extracted energy is stored in a storage capacitor C_{dc} whose voltage is DC. With CDE, the piezoelectric voltage varies during the energy extraction, meaning that an intermediate energy storage (such as an inductor) is required to transfer the energy to the constant voltage capacitor C_{dc}. Thus, in most CDE strategies, the harvesting process consists in temporarily storing energy from the harvester in the inductor, then transmitting it either to a storage capacitor or back to the harvester. The energy extracted during each vibration period is given by the area of the $(x\ v_p)$ cycle $E_{ext} = \oint x\, dv_p$.

The extracted power with CDE strategies is not intrinsically dependent on the voltage across the load capacitor C_{dc}. CDE tunable parameters consist in adjusting the value of the mechanical displacement right before the extraction. Some possible CDE tuning parameters are the frequency of the harvesting events f_{sw} [6], the phase of the harvesting events ϕ_{sw} with respect to the displacement extrema $\pm x_{max}$ [16], and the voltage inversion ratio β_{sw}—defined as the ratio between the piezoelectric voltage right after the harvesting event and the voltage right before the harvesting event [12][30]. Of course, this set of parameters is not exhaustive, and many others may be implemented.

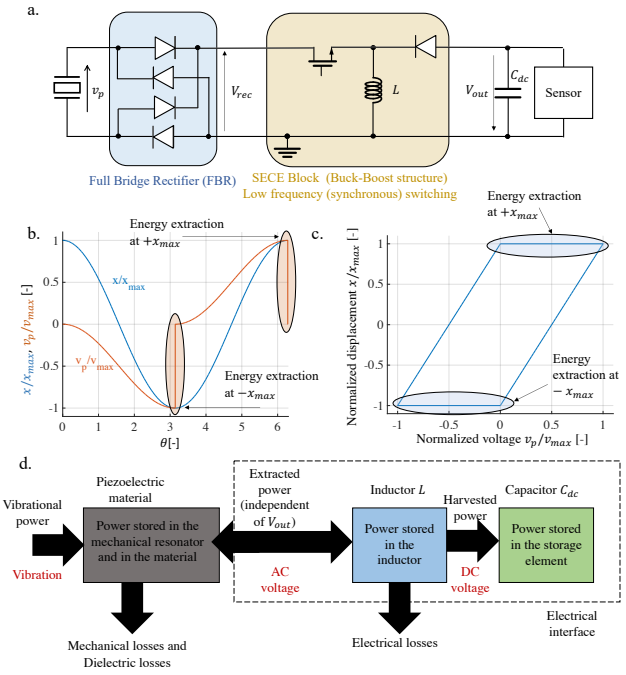

Figure 3.a. System implementation, b. normalized transient waveforms, c. $(x\ v_p)$ cycle of a CDE strategy (SECE), and d. power flow of a CDE strategy (SECE).

In the literature, most CDE analyses provide the expression of the extracted power [6][16][18] and the expression of the harvested power is usually derived in an ad-hoc, case-by-case manner [31]. However, as proven in [23], the electrical efficiency of CDE strategies can be approximated as a function of the voltage inversion ratio $\beta_{sw} \in [\beta_{min}, 1]$ and of the minimum inversion ratio β_{min} (closely related to the quality factor of the interface, Q_e, by $\beta_{min} = -e^{-\frac{\pi}{2Q_e}}$). The expression of this electrical efficiency is recalled by (12),

$$\eta_{elec}|_{CDE} = 1 - 2\frac{\arccos(\beta_{sw}) - \beta_{sw}\sqrt{1-\beta_{sw}^2}}{\pi\,(1-\beta_{sw}^2)(1-(\ln(-\beta_{min}))^{-1})} \quad (12)$$

where ln is the natural logarithm function. Combining (12) with CDE extracted power expressions, we can calculate the harvested power with any CDE, which can be compared with the harvested power with any CVE.

5.1.2 Constant Voltage Extraction Strategies

If the energy is extracted from the piezoelectric material with almost no variation of the voltage across the harvester, then the strategy will be classified as a Constant Voltage Extraction (CVE) strategy. A common interface that can be classified as a CVE is the PSSHI interface. Indeed, as shown in Figure 4, the

energy is extracted from the piezoelectric when the piezoelectric voltage v_p is approximately constant and equal to a DC voltage, $\pm V_{dc}$. The extracted energy during each period is given by the area of the $(x\ v_p)$ cycle $E_{ext} = \oint v_p\ dx$.

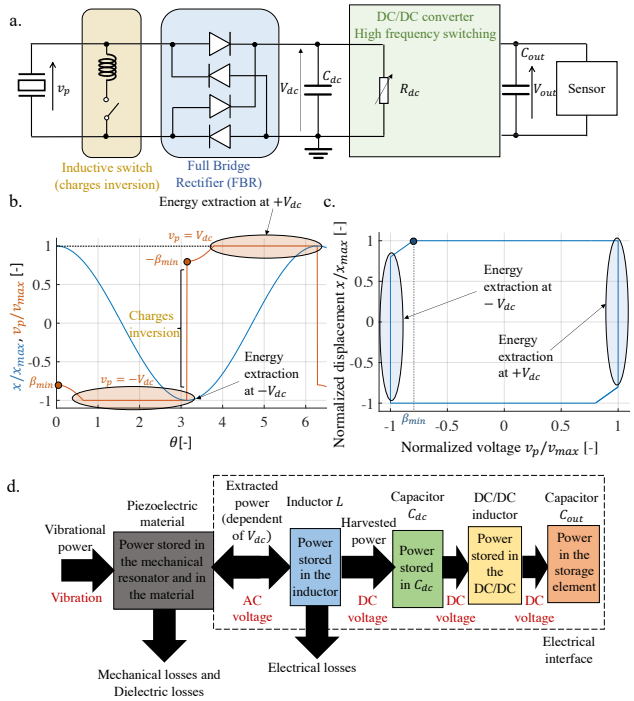

Figure 4. a Examples of a. system implementation, b. normalized transient waveforms, c. $(x\ v_p)$ cycle of a CVE strategy (PSSHI), and d. power flow of a CVE strategy (PSSHI).

The extracted power with CVE strategies is intrinsically dependent on the value of the extraction voltage V_{dc}. Since the voltage across the storage capacitance may vary with time if unregulated, it is necessary to find a way to adapt V_{dc}, making it independent from the voltage across the sensor V_{out}. In most cases, this fine-tuning is performed using a DC/DC converter in discontinuous current mode (DCM), as shown in Fig. 4. As detailed in [32], the input resistance of the DC/DC converter is then a function of the DC/DC duty-cycle and switching frequency, meaning that a control of the duty-cycle (or switching frequency) allows to tune V_{dc} to its optimal value. The choice of a tuning parameter which would not impact V_{dc}, while possible, is impracticable since this tuning parameter would have to compensate for any acceleration amplitude or V_{dc} changes. This is why all CVE in the literature, whether with one or two tuning parameters, include a tuning of V_{dc} [33][34]. The harvested power with any CVE can be simply expressed as (13),

$$P_{harv} = \frac{V_{dc}^2}{R_{dc}} \tag{13}$$

with R_{dc} being the equivalent impedance connected to C_{dc}, as shown in Fig. 4. The losses during the electrical charge inversion process are given by (14) (with $\beta_{sw} = \beta_{min}$ if all charges are reinjected as in PSSHI):

$$P_{loss} = \frac{\omega}{2\pi} C_p V_{dc}^2 (1 - \beta_{sw}^2) \tag{14}$$

Thus, from (13) and (14), we eventually find the electrical efficiency of CVE strategies:

$$\eta_{elec}|_{CVE} = \frac{P_{harv}}{P_{harv} + P_{loss}} = \frac{2\pi}{2\pi + \Omega\, r_{dc}(1 - \beta_{sw}^2)} \tag{15}$$

with $r_{dc} = R_{dc} C_p \omega_0$ the normalized load connected to C_{dc}. In the literature, analyses of CVE usually provide the expression of the harvested power P_{harv}, since its derivation can be relatively straightforward [33][34][35]. Note that (15) does not take into account the efficiency of the DC/DC converter (shown in Fig. 4), because the contribution of the DC/DC to the overall losses can be significantly reduced with appropriate design choices and transistor sizing.

5.1.3 Classification of well-known strategies as CDE/CVE

Figure 5 shows a classification of some well-known harvesting strategies depending on their families (CVE/CDE) and taking into account how many tuning parameters they allow.

Equation (8) combined with equations (15) (for CVE) or (12) (for CDE) leads to the harvested power envelopes (11) of all the CVE and CDE strategies as long as we know their electrical damping ε_D and electrical stiffness ε_K expressions. The expressions of ε_D and ε_K of some existing CDE (red) and CVE (green) in the literature (shown in Fig. 5) have been gathered in Appendix C. Based on these expressions, we can compute the EIC of each strategy as well as their power envelopes. The following sections present these results for single-tuning strategies (SEH, SOR, PSSHI, SSECE, etc.) and multi-tuning strategies (SCSECE, FTSECE, PS-SSHI, etc.).

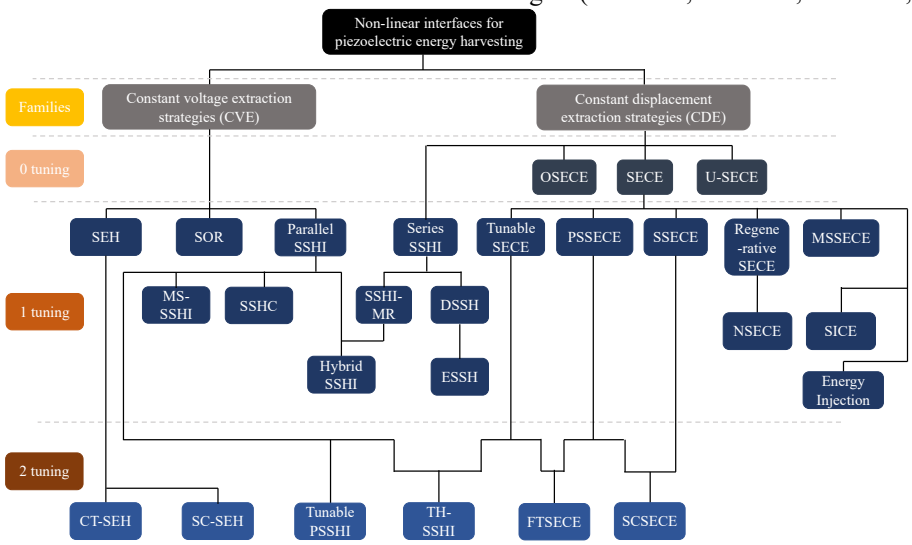

Figure 5. Classification of existing literature strategies. References of each strategy are given in Appendix C.

5.2 Single-tuning strategies

5.2.1 Single-tuning CVE

Most CVE strategies exhibiting a single tuning parameter can be gathered under three categories:

- SEH [33] (and SEH-like strategies) where there is no energy reinjected in the PEH.
- PSSHI and PSSHI-like strategies such as MS-SSHI [36], SSHC [11], SSHO [37], etc. where all the energy left in the piezoelectric material after the extraction is reinjected in the PEH ($\beta_{sw} = \beta_{min}$).
- SOR [38] (and SOR-like strategies) where all the energy left in the piezoelectric material after the energy extraction is quickly evacuated and transformed into heat ($\beta_{sw} = 0$).

For each strategy, the tuning parameter is the normalized load r_{dc} which controls the constant voltage V_{dc}. Figure 6 presents the power envelopes for a PEH exhibiting a quality factor $Q_m = 50$ and a coupling coefficient k_m^2 of 0.002 (Fig.6.a), 0.05 (Fig.6.b), and 0.3 (Fig.6.c). The minimum voltage inversion ratio β_{min} has been fixed to -0.8. In each case, we also observe in Fig.6 the optimal values of the electrical damping ε_D and stiffness ε_K associated with each strategy, and the values of these two parameters corresponding to the optimality criteria given by (4). For weakly coupled PEH (Fig.6.a), the harvested power is greater with PSSHI-like strategies than with SOR or SEH strategies. Indeed, the electrical damping induced by PSSHI ($\varepsilon_{D,\max}|_{PSSHI} = \frac{4}{\pi(1+\beta_{min})}$) is much larger than the electrical damping induced by the SEH or SOR ($\varepsilon_{D,\max}|_{SEH} = \frac{1}{\pi}$, $\varepsilon_{D,\max}|_{SOR} = \frac{4}{\pi}$). This explains why the PSSHI extracts more energy when the harvester is weakly coupled and/or strongly damped, since, in this case, maximizing the extracted energy requires maximizing the electrical damping. For weakly coupled PEH, tuning ε_K has little to no impact on the power envelopes. This explains why all the envelopes of Fig.6.a exhibit a single local extremum for $\Omega \approx 1$. This is why the literature on weakly coupled PEH interfaces focusses on maximizing the electrical damping while not considering (or even modelling) the electrical stiffness [38]. For stronger coupling values (Fig.6.b), the maximum of the power envelopes for each strategy are close to P_{lim}. Indeed, greater electromechanical coupling implies smaller optimal electrical damping (4). Figure 6.b. also shows that tuning ε_K for moderately coupled PEH is useful, as shown in the case of the SEH where ε_K follows $\varepsilon_{K,opt}$ on a small frequency band $\forall\Omega \in [1,1.03]$.

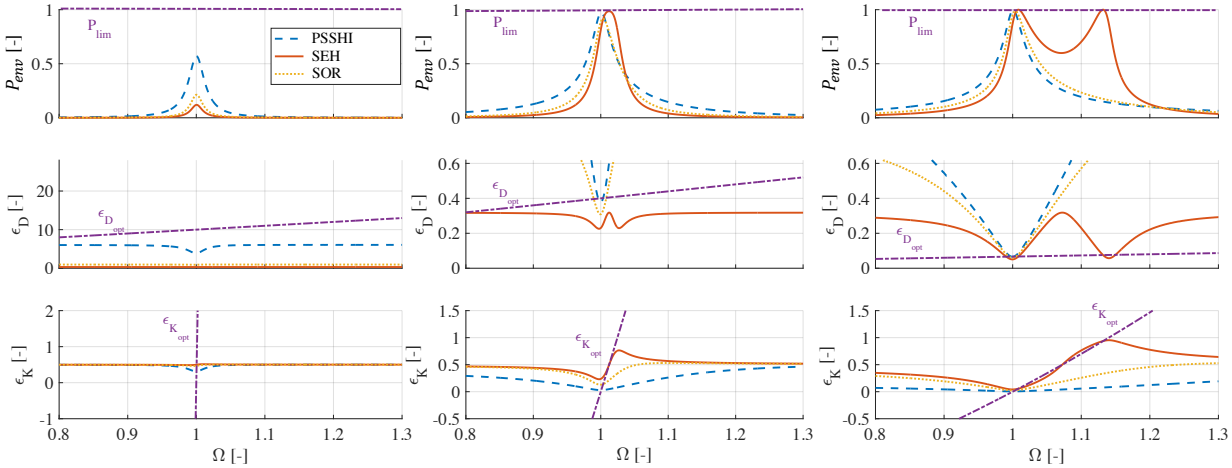

Figure 6. Harvested power envelopes of single-tuning CVE: SEH (red), SOR (yellow), PSSHI (blue), and P_{lim} (purple) with $Q_m = 50$, $\beta_{min} = -0.8$ and a. $k_m^2 = 0.002$ b. $k_m^2 = 0.05$ c. $k_m^2 = 0.3$.

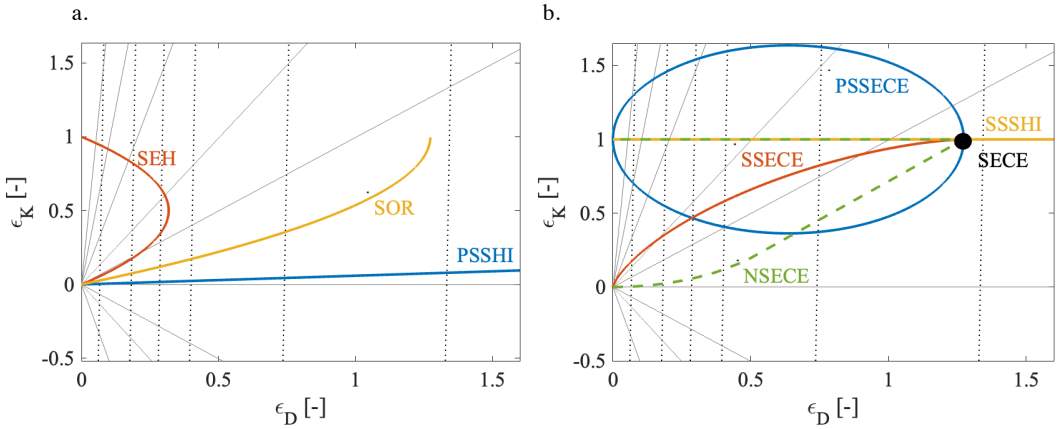

Figure 7. EIC of a. single-tuning CVE: SEH (red), SOR (yellow) and PSSHI (blue), b. single-tuning CDE: PSSECE (blue), NSECE (green), SSECE (red), and SSSHI (yellow).

In the case of strongly coupled PEH (Fig.6.c), each extraction strategy allows to extract P_{lim} for one (PSSHI and SOR) or two (SEH) vibration frequencies. Any further increase of the coupling would not result in a harvested power beyond P_{lim}. However, a stronger coupling opens doors for the tuning of both ε_D and ε_K, leading to a larger harvesting bandwidth and an increased robustness to shifts of the vibration frequency. We note that the ε_K of SEH, contrarily to the ε_K of SOR or PSSHI, remains in the vicinity of $\varepsilon_{K,opt}$ on a relatively large frequency band $\forall\Omega \in [1,1.15]$. Hence, associated with a strongly coupled and/or weakly damped PEH, SEH reaches a broader harvesting bandwidth than SOR and PSSHI. The possible electrical influences $\left(\varepsilon_D(r_{dc}), \varepsilon_K(r_{dc})\right)$ of single-tuning CVE (SEH, PSSHI and SOR) have been computed on the EIC shown in Fig. 7.a. Even though PSSHI reaches large values of ε_D - which explains its effectiveness with weakly coupled and/or strongly damped PEH - its representation $\varepsilon_K(\varepsilon_D)$ only crosses each dashed line (representing the optimal couples $(\varepsilon_D,\ \varepsilon_K)$ for a given PEH) a single time. This explains why there is only a single vibration frequency where the extracted power of PSSHI is equal to P_{lim}. On the other hand, the maximum reachable value of ε_D with SEH is only π^{-1}, which explains why the performances of SEH with a weakly coupled and/or highly damped PEH are limited. However, for strongly coupled and/or weakly damped PEH, the SEH representation $\varepsilon_K(\varepsilon_D)$ crosses each dashed line twice. This explains why the SEH power envelope exhibits two local maxima of power [39] above a certain electromechanical coupling.

5.2.2 Single-tuning CDE

We also group existing single-tuning CDE under four categories, depending on their tuning parameter and their voltage waveforms:

- PSSECE [16] (and PSSECE-like strategies) whose tunable parameter is the phase between the voltage extrema and the energy extraction.
- SSECE [17] (and SSECE-like strategies) whose tunable parameter is the duration of a short-circuit sequence.
- NSECE [6] (and NSECE-like strategies) whose tunable parameter is the energy extraction frequency.
- Series SSHI (SSSHI) [40] and all the other strategies that allow a tuning of β_{sw}: tunable SECE [30], DSSH [41], ESSH [42], SSHI-MR [43], etc.

Figure 8 depicts the harvested power envelopes of these four groups of strategies for a PEH having a quality factor $Q_m = 50$ and an electromechanical coupling k_m^2 of 0.002 (Fig.8.a), 0.05 (Fig.8.b), and 0.3 (Fig.8.c). The minimum voltage inversion ratio β_{min} has been fixed to -0.8.

As expected, for PEH exhibiting a low $k_m^2 Q_m$, the harvested power is sensibly larger for the Series SSHI strategy than for the SECE-based interfaces. Similarly to what has been said for CVE interfaces, to optimize the extracted power for weakly coupled/strongly damped harvesters, maximizing ε_D prevails over tuning ε_K. This explains why all the power frequency responses exhibit a single global extremum for $\Omega_m \approx 1$. As the coupling gets larger, the maximum power of all the tunable CDE strategies becomes close to P_{lim}.

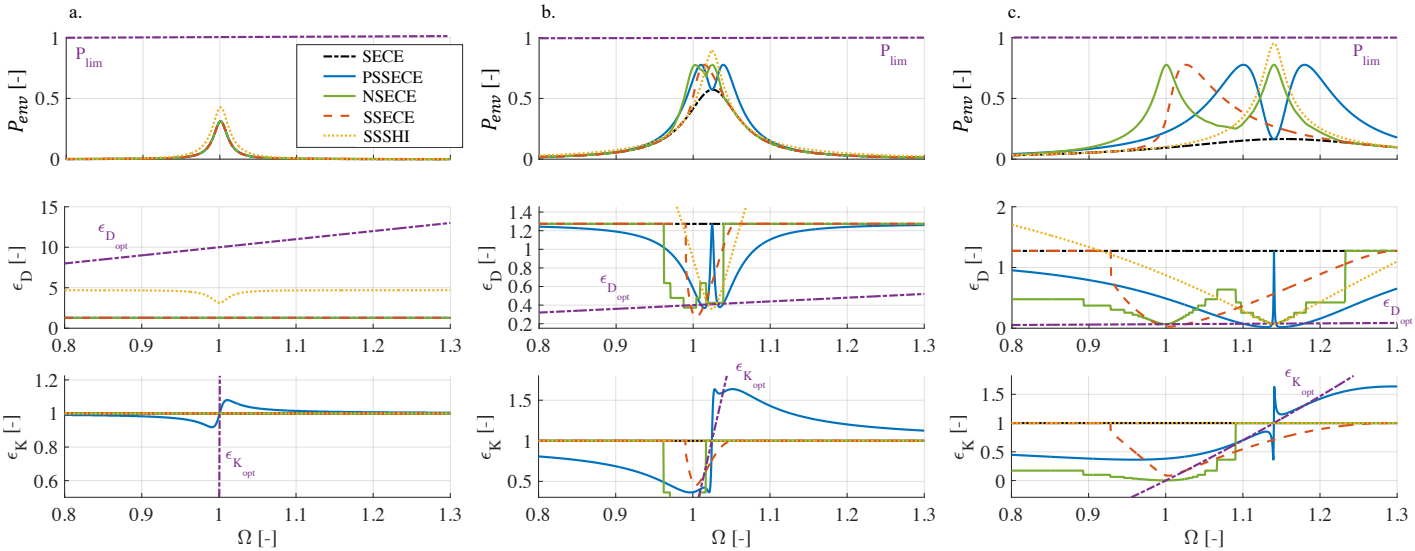

Figure 8. Harvested power envelopes of SECE (black) and of single-tuning CDE: PSSECE (blue), NSECE (green), SSECE (red), SSSHI (yellow), and P_{lim} (purple) with $Q_m = 50$, $\beta_{min} = -0.8$, and a. $k_m^2 = 0.002$ b. $k_m^2 = 0.05$ c. $k_m^2 = 0.3$. The harvested power envelopes of SECE, NSECE, PSSECE, have already been validated experimentally in [19] [6] [16].

As depicted in Fig.8.c, for large values of k_m^2, the bandwidths of PSSECE, SSECE and NSECE become significantly larger compared to the bandwidth of Series SSHI. Which of these three strategies exhibits the broadest harvesting bandwidth remains an open question (which will be discussed in the 6th section of this paper). However, one may notice that both NSECE and PSSECE exhibit two power maxima against a single one for SSECE, making them good candidates for harvesting energy on wide frequency bands.

Figure 7.b shows the reachable values of $(\varepsilon_D, \varepsilon_K)$ for the single-tuning CDE. For weakly coupled harvesters (right side of the plane), the only CDE that is able to reach P_{lim} is the Series SSHI due to the important value of $\max(\varepsilon_{D_{S-SSHI}})$. However, the drawback of the Series SSHI can clearly be observed in Fig. 7.b: it is modeled as a horizontal line with a constant electrical stiffness ($\varepsilon_{K_{SSSHI}} = 1$), which shows its inability to tune the PEH resonance frequency. For strongly coupled harvesters (left side of the plane), all strategies are able to reach P_{lim}, for a single frequency with Series SSHI and SSECE, and two frequencies with PSSECE and NSECE. We can also observe that PSSECE exhibits the largest range of ε_K, going from $1 - 2/\pi$ to $1 + 2/\pi$, larger than the ε_K ranges of the SSECE and NSECE which both go from 0 to 1.

5.3 Multi-tuning strategies

This section focuses on double-tuning electrical strategies, that can control ε_D and ε_K independently (on a defined frequency range) by means of two tunable parameters, ψ_1 and ψ_2. As shown in Fig.7, an interface with no tuning (such as the SECE strategy) can be represented as a single dot on the EIC, while a single-tuning interface can be represented as a smooth curve $\mathcal{C}_{strategy}$ (association of single dots). Thus, the representations of multiple-tuning interfaces ($k \geq 2$) in the EIC are surfaces $\mathcal{S}_{strategy}$ (association of smooth curves).

There are a few strategies in the literature that combine two tuning parameters: the TH-SSHI, the FTSECE, the SCSECE, and the PS-SSHI. Figure 9 presents the surface representations of these four strategies in the EIC. We can observe that the surfaces corresponding with the PS-SSHI and FTSECE are similar and particularly large. The diameter of their disk representation depends on the maximum ε_D reachable with each strategy, hence it is directly linked with β_{min}. In both cases, this diameter is equal to $\frac{4}{\pi}\frac{1-\beta_{min}}{1+\beta_{min}}$. In the case of a lossless interface ($\beta_{min} \to -1, \eta_{elec} \to 1$), the surfaces of the FTSECE and PS-SSHI tend toward infinity. Figure 9 proves that both the FTSECE and PS-SSHI maximize the extracted power on a large frequency band. However, as discussed previously in this paper and in [23], there is a difference between extracted power and harvested power (the latter taking the electrical efficiency into account). Since the electrical efficiency decreases with a greater inversion (or a lower β_{sw}), the difference between extracted power and harvested power can be particularly important for the FTSECE and PS-SSHI. Figure 10 illustrates the harvested power envelopes of these four strategies for a PEH having a quality factor $Q_m = 50$ and an electromechanical coupling k_m^2 of 0.002 (Fig.10.a), 0.05 (Fig.10.b), and 0.3 (Fig.10.c). For weakly coupled PEH, the PS-SSHI and TH-SSHI allow to harvest more power than the FTSECE and SCSECE. Indeed, while all PS-SSHI, TH-SSHI, and FTSECE reach the same maximum value of ε_D (leading to the same extracted power), the electrical efficiencies of PS-SSHI and TH-SSHI are more important than FTSECE, which explains the difference in harvested power. The SCSECE, associated with a weakly coupled PEH, harvests less power than the other ones because of the relatively low value of $\max(\varepsilon_D) = 4/\pi$. For strongly coupled PEH, Fig.10 shows that PS-SSHI and FTSECE power envelopes do not share the same shape. The global extremum of each envelope is reached for a different vibration frequency ($\Omega = 1$ for PS-SSHI and $\Omega = 1.14$ for FTSECE) even though their representations in the EIC are almost identical (Fig.9). Indeed, the electrical efficiency of PS-SSHI is maximized around the short-circuit resonance frequency of the PEH ($\Omega_{sc} = 1$) while the electrical efficiency of FTSECE is maximized around the open-circuit resonance frequency of the PEH ($\Omega_{oc} = \sqrt{1 + k_m^2}$). The power envelopes of TH-SSHI presents a valley between these two frequencies that can be understood from the unreachable couples $(\varepsilon_D, \varepsilon_K)$ in Fig. 9.b. Finally, SCSECE exhibits an interesting power envelope, even though its surface on the EIC is limited (Fig.9.a). The electrical efficiency of SCSECE is constant ($\beta_{sw} = 0\ \forall\Omega$), which explains why its power envelope exhibits a plateau for $\Omega \in [0.98, 1.19]$. The harvesting bandwidth of the SCSECE is the largest: $\Delta\Omega_{\mathrm{SCSECE}} = 0.29$ against $\Delta\Omega_{\mathrm{FTSECE}} = 0.20$, $\Delta\Omega_{\mathrm{PS-SSHI}} = 0.17$ and $\Delta\Omega_{\mathrm{TH-SSHI}} = 0.18$. On the other hand, the maximum value of the SCSECE power envelope is also the smallest, peaking at $0.78P_{\mathrm{lim}}$.

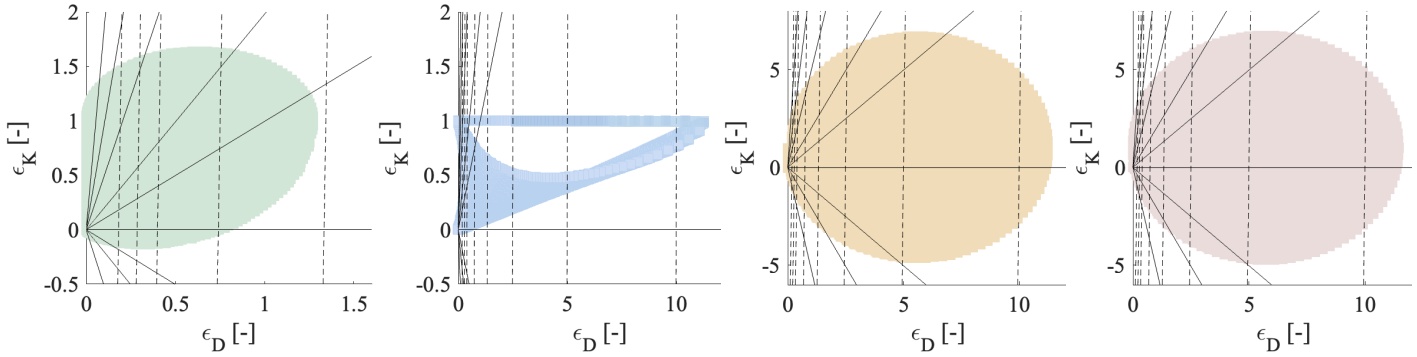

Figure 9. Electromechanical influences charts of double-tuning strategies: a. SCECE, b. TH-SSHI, c. FTSECE and d. PS-SSHI.

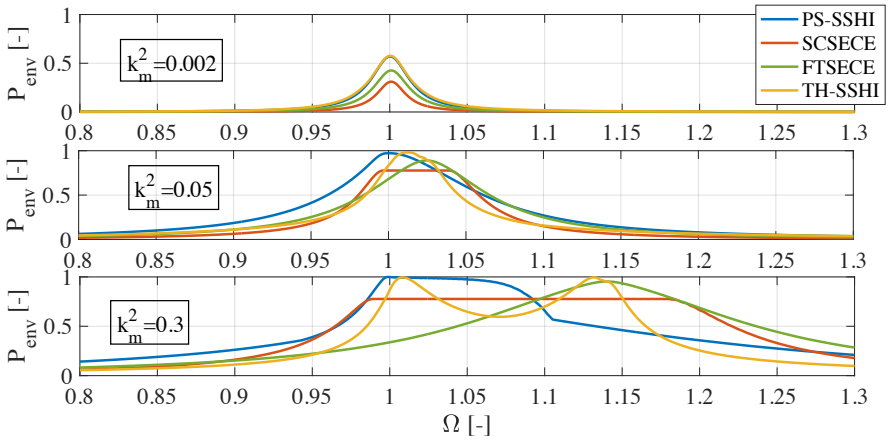

Figure 10. Harvested power envelopes of the PS-SSHI (blue), SCSECE (red), FTSECE (green), and TH-SSHI (yellow), with $Q_m = 50$, $\beta_{min} = -0.8$ and a. $k_m^2 = 0.002$ b. $k_m^2 = 0.05$ c. $k_m^2 = 0.3$. The power envelopes have been validated experimentally in [19] [18] [22].

6. Quantitative comparisons of tunable strategies

6.1 A quantitative criterion for evaluating strategies

In the previous sections, we were able to represent each strategy with normalized and unifying tools such as the electromechanical influences chart and the power envelope. However, while there exists a quantitative criterion for determining the best strategy associated with weakly coupled PEH (the maximum value of the electrical damping), choosing the best strategy for moderately and strongly coupled PEH remains a tough issue. Indeed, from Fig.10, one might hardly determine which strategy is the best among the FTSECE, PS-SSHI, or SCSECE. Furthermore, all simulations in the previous sections were run with a fixed $\beta_{min} = -0.8$ (fixed electrical quality factor). With a better (or poorer) quality interface, the conclusions on the best interface would be fundamentally different. For all these reasons, this section defines a quantitative criterion, in order to compare strategies for any PEH coupling and any value of β_{min}. This criterion, named χ_{comp} is defined by (16).

$$\chi_{comp} = \frac{\int_0^\infty P_{env,strat}(\Omega)\mathrm{d}\Omega}{\int_0^\infty P_{ref}(\Omega)\mathrm{d}\Omega} \tag{16}$$

A strategy's χ_{comp} is defined as the integral of the harvested power envelope, normalized by the integral of a reference envelope noted P_{ref}. This reference envelope corresponds to the harvested power envelope of a PEH associated with a strategy with no tunable parameter ($k = 0$) and no electrical losses ($\eta_{elec} = 1$). Furthermore, P_{ref} reaches P_{lim} for $\Omega = 1$ (meaning that $\varepsilon_K|_{ref} = 0$ and $\varepsilon_D|_{ref} = 1/(k_m^2 Q_m)$). The analytical expression of this reference envelope can be obtained from (8) and is given by (17).

$$P_{ref} = \frac{4\Omega}{\left(Q_m(1-\Omega^2)\right)^2 + (\Omega+1)^2} \tag{17}$$

χ_{comp} is dimensionless and depends on three factors: k_m^2 and Q_m that both quantify the "quality" of a PEH, and β_{min} that quantifies the "quality" of the inversion/transfer of electrical charges in the interface circuit. These dependencies are in agreement with the conclusions that were drawn from the previous sections of this paper: the performances of an electrical strategy depend both on the coupling and on the quality factor of the PEH, as well as on the quality of the electrical interface.

6.2 Quantitative comparison of electrical strategies

Figure 11.a presents the χ_{comp} of all the single-tuning strategies presented in this paper as a function of k_m^2, with $Q_m = 50$ and $\beta_{min} = -0.8$. SSHI strategies (SSSHI and PSSHI) exhibit the highest χ_{comp} when the PEH is weakly coupled. Indeed, because they reinject electrical charges in the harvester ($\beta_{sw} < 0$), they exhibit high electrical damping values leading to important extracted power with weakly coupled PEH. SECE (and other CDE having a $\beta_{sw} = 0$ such as NSECE, PSSECE, and SSECE) are relatively efficient with weak coupling PEH, because their electrical damping is relatively strong ($\max(\varepsilon_D) = 4/\pi$). Finally, SEH is the least efficient strategy with weakly coupled PEH, because its electrical damping always remains below $1/2$. These results underline the correlation between energy re-injection (β_{sw} value), maximal value of the electrical damping ($\max(\varepsilon_D)$) and performances of an electrical strategy associated with weak coupling PEH.

As the coupling gets stronger, the increase of χ_{comp} for SSHI strategies and SOR slows down. Indeed, as shown previously, these strategies do not enable a tuning of the electrical stiffness while keeping the electrical damping optimal. Hence, they make poor use of stronger coupling and their harvesting bandwidth remains relatively constant for any k_m^2. On the other hand, the χ_{comp} of SECE-based strategies (NSECE, SSECE, PSSECE) and SEH (which provide good control of ε_K over a small range of ε_D) outmatch the SSHI strategy's χ_{comp} when the coupling is strong enough. The single-tuning strategy that maximizes χ_{comp} for strongly coupled PEH is the PSSECE, which is understandable since:

- Its ε_K range of variation is the largest among the single-tuning strategies.
- Its power envelope exhibits two local maxima.

One may notice that a larger coupling always leads (except in the case of SECE) to a higher χ_{comp}, meaning that selecting the best coupling mode (usually 3-1 mode for cantilever-type harvesters) and optimizing the dimensions of the harvester in order to maximize k_m^2 is extremely important [14].

Figure 11.b presents the χ_{comp} of all the double tuning strategies presented in this paper as a function of k_m^2, with $Q_m = 50$ and $\beta_{min} = -0.8$. In weak coupling cases, the best strategies are, again, the ones that exhibit the largest electrical damping: TH-SSHI, CT-PSSHI, and PS-SSHI. Comparing Fig.11.b with Fig.11.a, we notice that the χ_{comp} of TH-SSHI and PS-SSHI are sensibly the same as the χ_{comp} of PSSHI. Indeed, adding a second tuning parameter has little to no use if the PEH coupling is weak. When the PEH coupling gets stronger ($k_m^2 \in [0.01,0.2]$), we can observe in Fig.11.b that PS-SSHI still exhibits the largest χ_{comp}, closely followed by FTSECE. However, when k_m^2 exceeds 0.4, the strategy that maximizes χ_{comp} becomes SCSECE. The difference in terms of χ_{comp} between SCSECE and PS-SSHI/FTSECE continues to increase as the coupling gets stronger. The reason behind this result is that the electrical efficiency of SCSECE is constant for all frequencies and hence does not limit its harvesting bandwidth, contrary to FTSECE and PS-SSHI cases. Some capacitive tuning techniques (CT-PSSECE, CT-SEH) exhibit particularly good performances for strong coupling PEH due to their high range of ε_K and electrical efficiency which remains relatively high compared to strategies which require re-injecting energy (i.e., PS-SSHI and TH-SSHI that require a $\beta_{sw} < 0$). We can note that TH-SSHI performances are relatively low, which stem from its inability to control ε_D and ε_K independently on a large frequency range ("hole" in Fig.9.b).

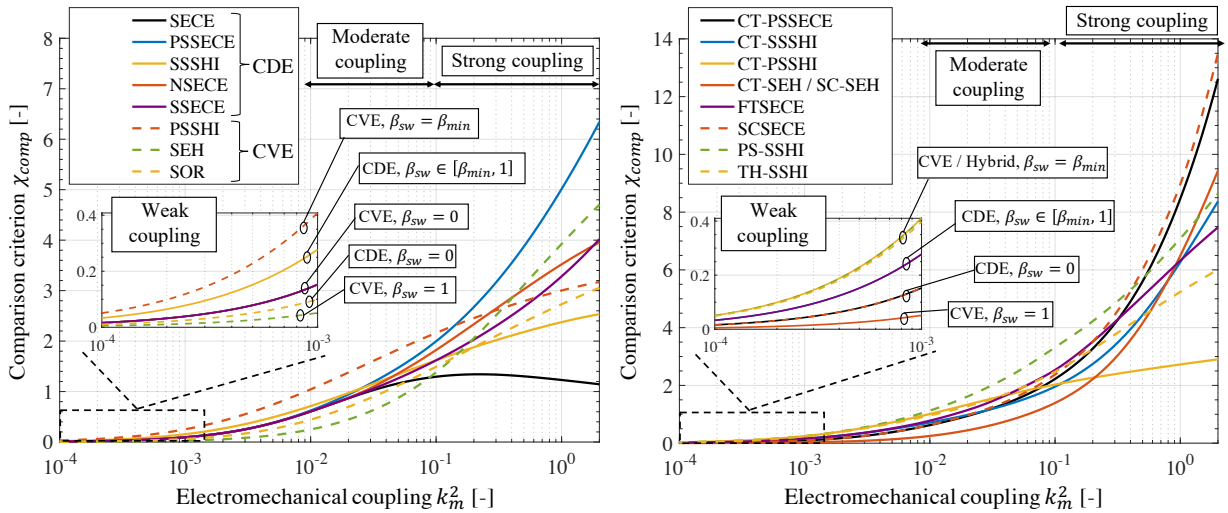

Figure 11. χ_{comp} of a. single-tuning CDE (solid lines) and CVE (dashed lines) and b. double-tuning strategies as a function of k_m^2 with $Q_m = 50$ and $\beta_{min} = -0.8$.

However, the results and conclusions obtained from Fig.11.a and Fig.11.b are not general because we supposed that the β_{min} of the interface was -0.8. While this is a relatively realistic value for β_{min}, some papers in the literature propose interfaces that go below this value by means of multiple discharges techniques [44] [36], clever engineering, and transistor sizing [45][46][47]. On the other hand, some interfaces relying on discrete components exhibit β_{min} that are larger than -0.8. The impact of β_{min} on the conclusions previously made will now be studied, in order to understand how β_{min} impacts the choice of the interface. Figure 12 presents the single-tuning strategies maximizing χ_{comp} as a function of k_m^2 and β_{min}.

For weakly coupled / strongly damped harvesters, the strategy maximizing χ_{comp} is PSSHI for any value of β_{min}. This result is in agreement with the conclusions made in the previous sections. If the PEH is strongly coupled / weakly damped and k_m^2 is greater than (approximately) 0.2, the best single-tuning strategy depends on the value of β_{min}. If the quality of the electrical interface is relatively good ($\beta_{min} < -0.7$), the strategy maximizing χ_{comp} is PSSECE, which is in agreement with the predictions made from Fig. 8 and Fig. 12. However, if the electrical interface exhibits heavy losses, ($\beta_{min} > -0.7$), the best strategy becomes SEH.

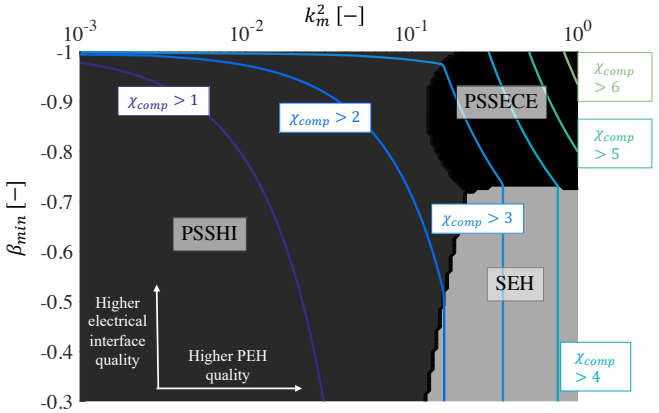

Figure 12. Single-tuning strategies maximizing χ_{comp} as a function of k_m^2 and β_{min} (with $Q_m = 50$).

Figure 13 presents the double tuning strategies maximizing χ_{comp} as a function of k_m^2 and β_{min}. We can note that the double-tuning strategies indicated in Fig. 13 will always exhibit an χ_{comp} equal or greater as the ones shown in Fig. 12. Adding a second tuning becomes particularly beneficial (i.e. χ_{comp} becomes 20% greater between Fig. 12 and Fig. 13) when $k_m^2 Q_m > 7(1+\beta_{min})$, as shown by the dashed red line on Fig. 13.

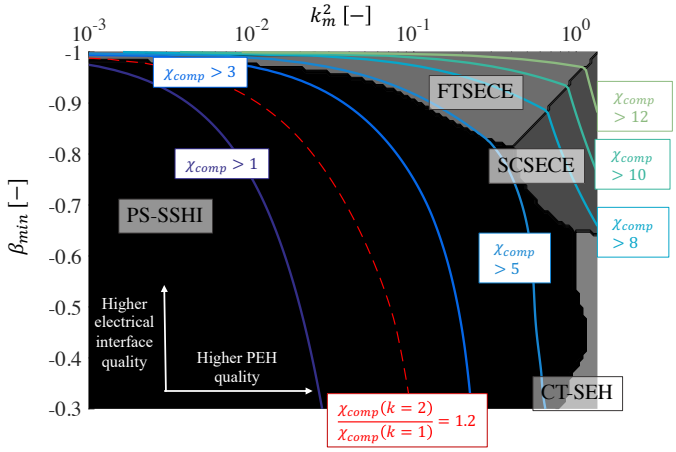

Figure 13. Double tuning strategies maximizing χ_{comp} as a function of k_m^2 and β_{min} (with $Q_m = 50$).

For weakly coupled / strongly damped harvesters, the strategy maximizing χ_{comp} is PS-SSHI for any value of β_{min}. For greater values of k_m^2, FTSECE becomes the best strategy as long as the electrical interface quality is good (β_{min} close to -1). When the product $k_m^2 Q_m$ is important, ($k_m^2 Q_m > 15$), the strategies maximizing χ_{comp} become SCSECE (if $\beta_{min} < -0.65$) and CT-SEH (and SC-SEH) (if $\beta_{min} > -0.65$).

6.3 Application of the proposed analysis

6.3.1 Choice of the best electrical strategy

In this section, we propose to apply the proposed analysis on two PEH from the literature in order to determine the best electrical interface to implement with these PEH. The first PEH (called PEH1), from [47], is a cantilever-beam ceramic-based weakly coupled PEH. The second PEH (called PEH2), from [48], is a strongly coupled PEH made with PZT stacks. Table 3 summarizes the parameters of these two PEH.

Table 3. Parameters of two PEH from the literature.

Parameters	PEH1 [47]	PEH2 [48]	Units
ω_0	474	952	[rad.s^{-1}]
P_{lim}	0.14[a]	30[b]	mW
$\boldsymbol{k_m^2}$	**0.008**	**0.094**	**[-]**
$\boldsymbol{Q_m}$	**92**	**110**	**[-]**
$\boldsymbol{k_m^2 Q_m}$	**0.74**	**10**	**[-]**

[a]Estimated from [47], for an acceleration of 1m.s^{-2}.
[b]From[48], for an acceleration of 0.2m.s^{-2}.

From Fig.12, because of its weak electromechanical coupling, the optimal single-tuning strategy associated with PEH1 is the PSSHI. From Fig.13, the optimal double tuning strategy is the PS-SSHI. Furthermore, because the low coupling of PEH1 positions it on the left of the red line in Fig.13, there is little-to-no interest in using double tuning strategies compared to single-tuning strategies. Therefore, in order to optimally collect energy from the PEH1, the designer should choose to implement the PSSHI strategy.

The electromechanical coupling of PEH2 is much stronger. The optimal single-tuning strategy for PEH2 depends on the quality of the electrical interface (value of β_{min}). With an inductor exhibiting important conductive losses such as the one in [18], the optimal single-tuning strategy with PEH is the SEH. In the other hand, if the inductor exhibits less losses (such as the one in [9]), the best single-tuning strategy is the PSSECE. In the case of double tuning strategies, in most cases, the best strategy is the PS-SSHI. If the interface exhibits very few losses ($\beta_{min} < 0.85$) for instance with an integrated custom design with low-loss inductors such as the one in [47], the best double tuning strategy becomes the FTSECE. Note that PEH2 is always on the right of the red line in Fig. 13, meaning that double tuning interfaces will greatly increase the performances of the harvesting system compared to single-tuning interfaces, at the cost of an increased complexity and self-power consumption. Therefore, in order to optimally collect the energy from PEH2, the designer should choose to implement either the PSSECE, the SEH, the FTSECE or the PS-SSHI, depending on the quality factor of the inductor, and on the tradeoff between additional tuning parameters and increased complexity.

6.3.2 Thermal stability, aging, and vibration frequency shifts

Using the expression of the normalized extracted power (8), the expressions of the electrical efficiency (12) and (15), and the expressions of the electrical damping and stiffness (Appendix C), it is possible to compute the harvested power envelopes that can be obtained with each PEH with any electrical interface. For example, the power envelopes of PEH1 and PEH2 associated with a few selected electrical strategies have been computed in Fig. 14 (for $\beta_{min} = -0.8$). From Fig. 14, we can verify that the best interfaces for PEH1 are PSSHI and PS-SSHI (as predicted by Fig. 12 and Fig.13). In the case of PEH2, the best single-tuning strategy is the PSSECE, and the best double tuning strategy is the PS-SSHI, which confirm the analysis of section 6.3.1.

Figure 14 enables the prediction of the harvested power if the vibration frequency shifts away from the PEH resonance frequency. For example, in the case of PEH1 associated with the PSSHI interface, the harvested power is around 127µW if the vibration frequency is 75.5Hz. If the vibration frequency shifts to 74Hz, the harvested power drops to 40µW (31.5% of the max. power for a frequency shift of 2%). In the case of PEH2 associated with the PS-SSHI interface, the harvested power is around 30mW if the vibration frequency is 152Hz. If the vibration frequency shifts to 160Hz, the harvested power drops to 15.4mW (51% of the max. power for a frequency shift of 5.3%). Therefore, this shows that PEH2 is less sensitive to frequency shifts due to its large k_m^2 and by mean of a multi-tuning electrical interface such as the PS-SSHI.

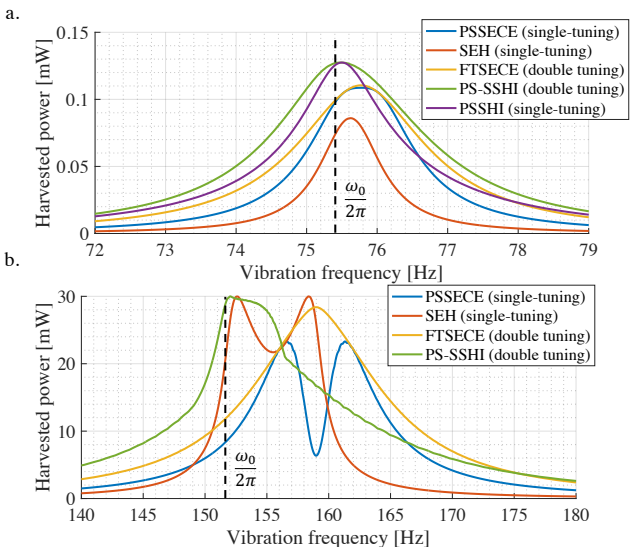

Figure 14. Power envelopes of a. PEH1 and b. PEH2 with various single- and multiple-parameters electrical strategies. $\beta_{min} = -0.8$.

Temperature variations might also be a cause for shifts in the PEH characteristics and mismatches between the harvester resonance frequency and the vibration frequency [27]. [49] shows that an increase of temperature (from 90°C to 120°C) leads to a shift of the resonance frequency from 1167Hz to 1108Hz (5.5% frequency shift) of a PZT-based harvester. In [50], the resonance frequency shifts from 290.4Hz to 281.8Hz (3% frequency shift) when the temperature is increased from 20°C to 100°C. A shift of the resonance frequency of the harvester has the same effect than a shift of the vibration frequency: in both cases, these shifts cause a mismatch between the vibration frequency and the resonance frequency. Therefore, the impact of such shift on the harvested power can be predicted from the power envelopes shown in Fig. 14. For example, if the resonance frequency of PEH2 shifts from 152Hz to 144.4Hz (5% frequency shift) due to temperature fluctuations, the harvested power can be estimated, from Fig. 14, to 15mW (50% decrease).

Note that an increase of the temperature might also lead to a decrease of the electromechanical coupling. [27] shows that increasing the temperature from 20°C to 100°C leads to a drop of hard PZT coupling coefficient of about 25%. Because of the dependency of the electromechanical coupling on the temperature, the best electrical strategy with a given PEH at 20°C might be different than the best electrical strategy with the same PEH at 120°C. Therefore, the designer should choose the electrical strategy that maximizes χ_{comp} considering the full range of temperature associated with the targeted application for its PEH. For example, in the case of PEH2, even if the electromechanical coupling gets lower due to temperature fluctuations, the best two-tuning electrical strategy, in most cases, remains the PS-SSHI.

Finally, aging might be another source of mismatch between the vibration frequency and the PEH resonance frequency. As detailed in [49], PEH resonance frequency might drop by a few percent (after millions of cycles) and then stabilize because of aging processes. The effects of aging on the harvested power can also be estimated using power envelopes (Fig.14), and can be minimized with an appropriate choice of electrical strategy.

6.3.3 Practical considerations concerning the electrical circuit

The analysis tools and comparisons (Fig. 12 and Fig. 13) proposed in this paper allow the designer to choose the best electrical strategy for a given PEH. However, the designer should also pay attention to a few practical considerations that have not been discussed in this paper:

i) If the coupling of the PEH is strong, the voltage across the piezoelectric elements tends to be large. Such large voltage can cause issues in terms of breakdown voltage in electronic components. This is particularly true in the case of ASIC implementation, where the breakdown voltage of integrated transistors can be relatively low (i.e., 10V as in [47]). On the one hand, if the voltage across the piezoelectric elements is too small (i.e., if the electromechanical coupling and the vibration amplitude are both weak), the electrical losses in the diodes of the interface circuit might completely hinder the performances of the harvester.

ii) If the resonance frequency of the PEH is too high, the efficiency of nonlinear circuit operating synchronously with the vibration frequency (such as SECE and SSHI circuits) might drop, because of the increase of switching losses.

iii) If the amplitudes of acceleration and voltage are too large, the mechanical resonator and the piezoelectric material (particularly if the PEH is made with polymers and composites) might start behaving nonlinearly, which is out-of-the-scope of the proposed analysis. The impacts of such nonlinearities should be evaluated by the designer in a case-by-case manner.

Note that, depending on the vibration characteristics, the energy can also happen to be provided in burst (for example for shock harvesting) [47], [51], [52]. For such applications, additional strategies should be considered to allow intermittent use at the power management level. Our study focusses on the optimization of the harvested power during the harvesting process, in situations where the time during which energy is available in the environment is long enough for the system to reach steady state.

7. Conclusion

As the performances and electromechanical coupling of PEH gradually increases as a result of progress in material sciences and mechanical design, adding tunability to the electrical interface seems to be an appropriate approach in order to electrically enhance the performance of energy harvesting solutions. The choice of the tuning parameters determines the tuning ability and should be carefully considered, depending on the characteristics of the mechanical harvester, the targeted range of vibrations frequencies, and other implementation constraints that arise when considering particular real-life applications.

In this work, we proposed a unified analysis of the impact of the electrical interface on the harvester's frequency response. We presented a comprehensive analysis of electrical strategies with various graphical and analytical tools, and provided a thorough comparison of these strategies. When harvesting energy from weakly coupled / strongly damped PEH, maximizing electrical damping is the most important design goal. In this case, Parallel, Series SSHI, and PS-SSHI are particularly well-adapted. When harvesting energy from strongly coupled / weakly damped PEH, the range of variation of the electrically induced stiffness as well as the shape of the power envelope become significant factors to consider. In this case, PSSECE and SEH (for single-tuning strategies) as well as SCSECE and FTSECE (for double-tuning strategies) are the most appropriate existing strategies. Thereafter, we applied the proposed analysis and tools to evaluate the performances of two PEH with various interface circuits, in order to find the best electrical strategy with each of these PEH. Finally, practical considerations such as thermal stability, frequency shifts, and aging, have been discussed.

The recent integration of tunable strategies with self-powered self-convergent ASIC makes it possible to design piezoelectric generators that adapt their own resonance frequency to their environments in real-time. Such solutions pave the way towards the industrialization of robust and optimized vibration energy harvesters that combine energy autonomy with decision autonomy.

References

[1] A. Brenes et al., "Maximum power point of piezoelectric energy harvesters: a review of optimality condition for electrical tuning," *Smart Materials and Structures,* 29, 033001, 2020.

[2] E.P. Jayakrishnan, J. Sayed, "Piezoelectric Energy Harvesting: A Review on Power Conditioning", in: George V., Roy B. (eds) *Advances in Control Instrumentation Systems*. Lecture Notes in Electrical Engineering, vol 660. Springer, Singapore, 2020.

[3] D. Guyomar, M. Lallart, "Recent Progress in Piezoelectric Conversion and Energy Harvesting Using Nonlinear Electronic Interfaces and Issues in Small Scale Implementation," *Micromachines*, 2, 274-294, 2011.

[4] A. Badel and E. Lefeuvre, "Nonlinear conditioning circuits for piezoelectric energy harvesters," Nonlinearity in Energy Harvesting Systems et. E Blokhina et al. (New York: Springer) pp 321-359, 2016.

[5] Y. Liao, H. A. Sodano, "Optimal parameters and power characteristics of piezoelectric energy harvesters with an *RC* circuit," in *Smart Material and Structures*, 18, 045011, 2009.

[6] A. Morel, A. Badel, Y. Wanderoild, and G. Pillonnet, "A unified N-SECE strategy for highly coupled piezoelectric energy scavengers," *Smart Mater. Struct.*, vol. 27, 084002, 2018.

[7] G. A. Lesieutre, G. K. Ottman, and H. F. Hofmann, "Damping as a result of piezoelectric energy harvesting," *Journal of Sound and Vibration*, vol. 269, no. 3, pp. 991–1001, Jan. 2004.

[8] G. K. Ottman, H. F. Hofmann, A. C. Bhatt, and G. A. Lesieutre, "Adaptive piezoelectric energy harvesting circuit for wireless remote power supply," *IEEE Transactions on Power Electronics*, vol. 17, no. 5, pp. 669–676, Sep. 2002.

[9] D. Guyomar, A. Badel, E. Lefeuvre, and C. Richard, "Toward energy harvesting using active materials and conversion improvement by nonlinear processing," *IEEE Transactions on Ultrasonics, Ferroelectrics, and Frequency Control*, vol. 52, no. 4, pp. 584–595, Apr. 2005.

[10] E. Lefeuvre, A. Badel, C. Richard, and D. Guyomar, "Piezoelectric energy harvesting device optimization by synchronous electric charge extraction," *J. Intell. Mater. Syst. Struct*., vol. 16, pp. 865–876, 2005.

[11] S. Du et al., "A Fully Integrated Split-Electrode SSHC Rectifier for Piezoelectric Energy Harvesting," in *IEEE Journal of Solid-State Circuits*, vol. 54, no. 6, pp. 1733-1743, June 2019, doi: 10.1109/JSSC.2019.2893525.

[12] A. Richter et al., "Tunable interface for piezoelectric energy harvesting," in *2014 IEEE 11th International Multi-Conference on Systems, Signals Devices (SSD14)*, pp. 1–5, 2014.

[13] H. Xia, Y. Xia, Y. Ye, L. Qian, G. Shi, and R. Chen, "Analysis and simulation of synchronous electric charge partial extraction technique forefficient piezoelectric energy harvesting," *IEEE Sensors J.*, vol. 18, no. 15, pp. 6235–6244, Aug. 2018.

[14] D. Gibus, et al., "Strongly coupled piezoelectric cantilevers for broadband vibration energy harvesting," *Applied Energy,* Vol. 277, 115518, 2020.

[15] N. A. Siddiqui, D.-J. Kim, R. A. Overfelt, and B. C. Prorok, "Electromechanical coupling effects in tapered piezoelectric bimorphs for vibration energy harvesting," *Microsyst. Technol*., vol. 23, no. 5, pp. 1537-1551, May 2017.

[16] E. Lefeuvre et al., "Power and frequency bandwidth improvement of piezoelectric energy harvesting devices using phase-shifted synchronous electric charge extraction interface circuit," *Journal of Intelligent Material Systems and Structures*, vol. 28, no. 20, pp. 2988-2995, Dec. 2017.

[17] A. Morel *et al*., "Fast-Convergence Self-Adjusting SECE Circuit With Tunable Short-Circuit Duration Exhibiting 368% Bandwidth Improvement," in *IEEE Solid-State Circuits Letters*, vol. 3, pp. 222-225, 2020, doi: 10.1109/LSSC.2020.3012340.

[18] A. Brenes *et al*., "Large-bandwidth piezoelectric energy harvesting with frequency-tuning synchronized electric charge extraction," in *Sensors & Actuators A,* 302, 111759, 2020.

[19] A. Morel, G. Pillonnet, P. Gasnier, E. Lefeuvre, and A. Badel, "Frequency tuning of piezoelectric energy harvesters thanks to a short-circuit synchronous electric charge extraction," *Smart Mater. Struct.,* Vol. 28, no 2. 025009, 2019.

[20] P. Hsieh, C. Chen and H. Chen, "Improving the Scavenged Power of Nonlinear Piezoelectric Energy Harvesting Interface at Off-Resonance by Introducing Switching Delay," in *IEEE Transactions on Power Electronics*, vol. 30, no. 6, pp. 3142-3155, June 2015, doi: 10.1109/TPEL.2014.2334611.

[21] B. Zhao, J. Liang and K. Zhao, "Phase-Variable Control of Parallel Synchronized Triple Bias-Flips Interface Circuit towards Broadband Piezoelectric Energy Harvesting," *2018 IEEE International Symposium on Circuits and Systems (ISCAS)*, 2018, pp. 1-5, doi: 10.1109/ISCAS.2018.8351800.

[22] A. Morel et al., "A Tunable Hybrid SSHI Strategy for Piezoelectric Energy Harvesting with Enhanced Off-resonance Performances," Journal of Physics: Conference Series PowerMEMS 2018, Vol. 1407, 012060, 2019.

[23] A Morel et al., "Electrical Efficiency of SECE-based Interfaces for Piezoelectric Vibration Energy Harvesting," *Smart Materials and Structures,* In press, 2021.

[24] Wang X, "Frequency Analysis of Vibration Energy Harvesting Systems," (London: Elsevier), 2016.

[25] J. Liang, H. Shu-Hung Chung, W.-H. Liao, "Dielectric loss against piezoelectric power harvesting," *Smart Mater. Struct.*, **23,** 092001, 2014.

[26] D. Gibus et al., "Non-linear losses study in strongly coupled piezoelectric device for broadband energy harvesting," *Mechanical Systems and Signal Processing*, in press, 2021.

[27] S.-B. Kim, J.-H. Park, H. Ahn, D. Liu, D.-J. Kim, "Temperature effects on output power of piezoelectric vibration energy harvesters", *Microelectronics journal*, vol. 42, pp. 988-991, 2011.

[28] B. Ahmed-Seddik et al., "Self-powered resonant frequency tuning for Piezoelectric Vibration Energy Harvesters," Journal of Physics, Conference Series PowerMEMS 2013, Vol. 476, 012069, 2013.

[29] Y. Liao, "Analysis of power and efficiency of piezoelectric vibration energy harvesters through an impedance plot," *Journal of Intelligent Material Systems and Structures*, Vol. 30, 20, pp. 3036-3055, 2019.

[30] E. Lefeuvre, A. Badel, A. Brenes et al., "Analysis of piezoelectric energy harvesting system with tunable SECE interface," *Smart Mater. Struct.*, vol. 26, no. 3, 2017.

[31] C. Chen, B. Zhao, and J. Liang, "Revisit of synchronized electric charge extraction (SECE) in piezoelectric energy harvesting by using impedance modeling," in *Smart Materials and Structures*, vol. 28, 10, 105053, 2019.

[32] E. Lefeuvre, D. Audigier, C. Richard, D. Guyomar, "Buck-Boost Converter for Sensorless Power Optimization of Piezoelectric Energy Harvester," *IEEE Transactions on Power Electronics*, vol. 22, no. 5, pp. 2018-2025, 2007.

[33] Y.C. Shu, I.C. Lien, "Analysis of power output for piezoelectric energy harvesting systems," *Smart Mater. Struct*., vol. 15, pp. 1499-1512, 2016.

[34] Y.C. Shu, I.C. Lien, and W. Wu, "An improved analysis of the SSHI interface in piezoelectric energy harvesting," *Smart Mater. Struct*., vol. 16, pp. 2253-2264, 2007.

[35] A. Morel et al., "Active AC/DC control for wideband piezoelectric energy harvesting," Journal of Physics: Conference Series PowerMEMS 2016, Vol. 773, 012059, 2016.

[36] J. Liang, Y. Zhao and K. Zhao, "Synchronized Triple Bias-Flip Interface Circuit for Piezoelectric Energy Harvesting Enhancement," in *IEEE Transactions on Power Electronics*, vol. 34, no. 1, pp. 275-286, Jan. 2019, doi: 10.1109/TPEL.2018.2815922.

[37] M. Lallart, W. Wu, L. Yan and S. Hung, "Inductorless Synchronized Switch Harvesting Using a Piezoelectric Oscillator," in *IEEE Transactions on Power Electronics*, vol. 35, no. 3, pp. 2585-2594, March 2020.

[38] Y. K. Ramadass and A. P. Chandrakasan, "An Efficient Piezoelectric Energy Harvesting Interface Circuit Using a Bias-Flip Rectifier and Shared Inductor," in *IEEE Journal of Solid-State Circuits*, vol. 45, no. 1, pp. 189-204, Jan. 2010.

[39] Y. Liao, J. Liang, "Unified modeling, analysis, and comparison of piezoelectric vibration energy harvesters," *Mechanical Systems and Signal Processing*, Vol. 123, pp. 403-425, 2019.

[40] I.C. Lien, Y.C. Shu, W.J. Wu, S.M. Shiu, and H.C. Lin, "Revisit of series-SSHI with comparisons to other interfacing circuits in piezoelectric energy harvesting," *Smart Mater. Struct*., vol. 19, no. 12, p. 125009, Dec 2010.

[41] M. Lallart, L. Garbuio, L. Petit, C. Richard, and D. Guyomar, "Double Synchronized Switch Harvesting (DSSH): A new energy harvesting scheme for efficient energy extraction," *IEEE Trans. Ultrason. Ferroelectr., Freq. Control*, vol. 55, no. 10, pp. 2119-2130, Oct. 2008.

[42] H. Shen, J. Qiu, H. Ji, K. Zhu, M. Balsi, "Enhanced synchronized switch harvesting: a new energy harvesting scheme for efficient energy extraction," *Smart Mater. Struct*., vol. 19, 115017, 2010.

[43] L. Garbuio, M. Lallart, D. Guyomar, C. Richard and D. Audigier, "Mechanical Energy Harvester With Ultralow Threshold Rectification Based on SSHI Nonlinear Technique," in IEEE Transactions on Industrial Electronics, vol. 56, no. 4, pp. 1048-1056, April 2009, doi: 10.1109/TIE.2009.2014673.

[44] K. Zhao, J. Liang and H. Wang, "Series Synchronized Triple Bias-Flip (S-S3BF) Interface Circuit for Piezoelectric Energy Harvesting," *2019 IEEE International Symposium on Circuits and Systems (ISCAS)*, pp. 1-5, 2019.

[45] D. A. Sanchez, J. Leicht, F. Hagedorn, E. Jodka, E. Fazel and Y. Manoli, "A Parallel-SSHI Rectifier for Piezoelectric Energy Harvesting of Periodic and Shock Excitations," in *IEEE Journal of Solid-State Circuits*, vol. 51, no. 12, pp. 2867-2879, Dec. 2016.

[46] Y. Cai and Y. Manoli, "A Piezoelectric Energy-Harvesting Interface Circuit with Fully Autonomous Conjugate Impedance Matching, 156% Extended Bandwidth, and 0.38μW Power Consumption," in *proc. IEEE International Solid State Circuit Conference*, pp. 148-150, 2018.

[47] A. Morel *et al*., "A Shock-Optimized SECE Integrated Circuit," in *IEEE Journal of Solid-State Circuits*, vol. 53, no. 12, pp. 3420-3433, Dec. 2018.

[48] Y. Kuang, Z. J. Chew, J. Dunville, J. Sibson, and M. Zhu, "Strongly coupled piezoelectric energy harvesters: Optimised design with over 100 mW power, high durability and robustness for self-powered condition monitoring", Energy Conversion and Management, 237, 2021.

[49] P. Gasnier et al., "A 120°C 20G-compliant vibration energy harvester for aeronautic environments", J. Phys.: Conf. Ser. **1407**, 012118, 2019.

[50] C. Borzea, A. Morega, D. Comeagă and Y. Veli, "Temperature Influence on the Performances of a PZT-5H Piezoelectric Harvester," *2021 12th International Symposium on Advanced Topics in Electrical Engineering (ATEE)*, 2021.

[51] H. Liu, Z. Ji, T. Chen, L. Sun, S. C. Menon and C. Lee, "An Intermittent Self-Powered Energy Harvesting System From Low-Frequency Hand Shaking," in *IEEE Sensors Journal*, vol. 15, no. 9, pp. 4782-4790, Sept. 2015.

[52] G. Yang, B. H. Stark, S. J. Hollis and S. G. Burrow, "Challenges for Energy Harvesting Systems Under Intermittent Excitation," in *IEEE Journal on Emerging and Selected Topics in Circuits and Systems*, vol. 4, no. 3, pp. 364-374, Sept. 2014.

[53] A. Brenes, E. Lefeuvre, A. Badel, S. Seok and C.-S. Yoo, "Unipolar synchronized electric charge extraction for piezoelectric energy harvesting," *Smart Mater. Struct.*, Vol. 27, no 7. 075054, 2018.

Appendix A - Power extraction limit of a linear PEH

The mean power that is extracted by the electrical interface can be expressed as (18).

$$P_{ext} = \frac{\Omega M \gamma_m^2}{k_m^2 2\pi\ \omega_0} \int_0^{2\pi/\Omega} U(\theta) I(\theta) d\theta \quad (18)$$

Considering that both U, X, and $\dot{X}$ are $2\pi/\Omega$ periodic, combining (2) with (18) leads to (19), as detailed in [1].

$$P_{ext} = -\frac{\Omega M \gamma_m^2}{2\pi\ \omega_0} \int_0^{2\pi/\Omega} \left[\dot{X}^2(\theta)/Q_m + \ddot{Y}(\theta)\dot{X}(\theta)\right] d\theta \quad (19)$$

Since both X and $\dot{X}$ are $2\pi/\Omega$ periodic, we can write $X = a_{X0} + \sum_{n=1}^{+\infty}(a_{Xn}\cos(n\Omega\theta) + b_{Xn}\sin(n\Omega\theta))$ as well as $\dot{X} = \Omega \sum_{n=1}^{+\infty} n(b_{Xn}\cos(n\Omega\theta) - a_{Xn}\sin(n\Omega\theta))$. Replacing these expressions in (19) and applying Parseval equality yields the expression of the extracted power with any harvesting strategy as a function of the displacement harmonics coefficients a_{Xn} and b_{Xn} (20).

$$P_{ext} = \frac{\Omega M \gamma_m^2}{2\ \omega_0} \left[\frac{a_{X1} B_f}{M} - \frac{\Omega}{Q_m}\left(\sum_{n=1}^{+\infty} n^2 X_n^2\right)\right] \quad (20)$$

With $X_n^2 = a_{Xn}^2 + b_{Xn}^2$ the squared magnitude of the n^{th} displacement harmonic. Equation (20) is maximized and is equal to the well-known power limit P_{lim} when the mechanical displacement harmonics respect the optimality conditions given by (21) [1].

$$\begin{cases} P_{ext} = P_{\text{lim}} = \dfrac{B_f^2 \gamma_m^2 Q_m}{8\ \omega_0 M} \\ a_{X1} = \dfrac{B_f Q_m}{2\Omega M} \\ \forall n > 1, b_{X1} = a_{Xn} = b_{Xn} = 0 \end{cases} \quad (21)$$

Appendix B – First-harmonic assumption

The first-harmonic assumption is a well-known consideration made in the analysis of energy harvesting interfaces in order to simplify the problem by only considering the impact of the fundamental component of the piezoelectric voltage on the dynamics of the system (and assuming that all the higher harmonics are filtered due to the large quality factor of the mechanical resonator) [4][18]. This section proposes a demonstration of this assumption in order to study non-linear interfaces and their impact on the dynamics of the harvester. By considering the expansion of the piezoelectric voltage $U = a_{U0} + \sum_{n=1}^{+\infty}(a_{Un}\cos(n\Omega\theta) + b_{Un}\sin(n\Omega\theta))$, (2) can be rewritten as follows:

$$\forall n \neq 1, \begin{cases} a_{Xn}(1 - n^2\Omega^2) + b_{Xn}\dfrac{n\Omega}{Q_m} = -a_{Un} \\ b_{Xn}(1 - n^2\Omega^2) - a_{Xn}\dfrac{n\Omega}{Q_m} = -b_{Un} \end{cases} \quad (22)$$

$$\begin{cases} a_{X1}(1 - \Omega^2) + b_{X1}\dfrac{\Omega}{Q_m} = -a_{U1} \\ b_{X1}(1 - \Omega^2) - a_{X1}\dfrac{\Omega}{Q_m} = -b_{U1} - 1 \end{cases} \quad (23)$$

From (22), the transfer function of the n^{th} harmonic given by $H_n = \frac{X_n}{U_n}$ $(\forall n > 1)$ can be expressed. Similarly, the expression of the transfer function of the fundamental given by $H_1 = \frac{X_1}{U_1}$ can be expressed from (23) if we assume that the conditions of optimality on a_{X1} and b_{X1} (21) are respected. The expression of H_n $(\forall n > 0)$ is given by (24).

$$\forall n > 0, H_n = \frac{X_n}{U_n} = \frac{1}{\sqrt{(1 - \Omega^2 n^2)^2 + \dfrac{n^2\Omega^2}{Q_m^2}}} \quad (24)$$

By considering that the vibration frequency will always remain relatively close to the resonance frequency of the vibration energy harvester, $\Omega = 1 + \delta\Omega$ (with $\delta\Omega \ll 1$), and by neglecting the higher order terms, we eventually find (25).

$$\begin{cases} H_1 = \dfrac{Q_m}{\sqrt{1 - 4Q_m^2\delta\Omega^2}} \\ \forall n > 1, \quad H_n = \dfrac{1}{n^2} \end{cases} \quad (25)$$

Combining (25) with (20) leads to a new expression of the extracted power:

$$P_{ext} = P_{\text{lim}}\left[1 - \frac{1}{Q_m^2}\sum_{n=2}^{+\infty}\left(\frac{\alpha_n}{n}\right)^2 - 4\,\delta\Omega^2 \sum_{n=2}^{+\infty}\left(\frac{\alpha_n}{n}\right)^2\right] \quad (26)$$

With $\alpha_n^2 = U_n^2/U_1^2$. (26) shows that the decrease of the extracted power from the voltage harmonics can be separated under two terms. The first one (in blue) can be considered negligible as long as the quality factor of the resonator is important. The second one (in green) can be considered negligible as long as the vibration frequency remains close to the resonance frequency of the harvester. These two assumptions can be considered true for most harvesters that exhibit relatively large quality factors $(Q_m > 20)$ and are usually excited around their resonance frequency $(\delta\Omega < 0.3)$. This proves that respecting the conditions of optimality on the fundamental mechanical displacement (21) is, in most cases, a sufficient condition to almost reach the power limit for any harvester, vibration frequency, and vibration magnitude. However, this demonstration also shows that we should pay attention to the impact of the harmonics if we consider further enlargements of the frequency bandwidth of linear energy harvesters that might lead to large values of $\delta\Omega$, even if the harvester exhibits a large quality factor.

Appendix C – Electrical damping and stiffness of well-known electrical strategies

The expressions of ε_D and ε_K of some existing CDE (red) and CVE (green) in the literature have been gathered in Table 4. The expressions of ε_D and ε_K for SC-SEH [35], PS-SSHI [20], and TH-SSHI [22] are given in the corresponding references since they cannot be contained in Table 4.

Note that the line CT-Strat (Capacitive Tuning Strategies) in Table 4 corresponds to any single tuning strategy with an additional tuning of a capacitance C_{para} placed in parallel with the piezoelectric element ($c = \frac{C_{para}}{C_{para}+C_p}$ is the dimensionless version of C_{par}). Additional details on capacitive tuning strategies are given in Appendix D.

Appendix D – Capacitive-tuning strategies

Adding a second tuning parameter to a single-tuning strategy can be easily done, by adding a tunable capacitance C_{para} in parallel with the piezoelectric material [28]. The tunable dimensionless parameter $c \in [0,1]$ is defined as $c = \frac{C_{para}}{C_{para}+C_p}$ with C_p being the piezoelectric capacitance. The effect of c on the smooth curves corresponding to the single-tuning strategies ($\mathcal{C}_{PSSECE}|_{c=0}$ for PSSECE, $\mathcal{C}_{SEH}|_{c=0}$ in the case of SEH) is a mathematical transformation, namely a directional scaling, with a scale factor of $(1-c, 1-c)$. This is particularly interesting since this capacitive tuning has the same effect on every single-tuning technique, due to the intrinsic linearity of this approach.

$$\begin{cases} \varepsilon_D|_{CT-strat}(\psi_1, c) = (1-c)\varepsilon_D|_{strat}(\psi_1) \\ \varepsilon_K|_{CT-strat}(\psi_1, c) = (1-c)\varepsilon_K|_{strat}(\psi_1) \end{cases} \quad (26)$$

Two examples of strategies are represented in the EIC in Fig.15: CT-PSSECE (PSSECE with an additional capacitive tuning) and CT-SEH (SEH with an additional capacitive tuning). All the reachable values of $(\varepsilon_D, \varepsilon_K)$ with these double-tuning strategies are displayed in light yellow. We can note that representing SC-SEH (Table 4, [35]) in the EIC would be strictly identical to the representation of CT-SEH shown in Fig.15. Despite the relative simplicity of the additional capacitive tuning, we can observe that the harvesting bandwidth reached at high coupling (Fig.16.c) is particularly large in the cases of CT-PSSECE, CT-SEH, and CT-SSHI. As predicted, the harvesting bandwidth of CT-PSSECE is, for a strongly coupled PEH, the most important one ($\max(\varepsilon_K) = 1 + 2/\pi$). The harvesting bandwidth of CT-SSSHI and CT-SEH are almost equal and relatively important ($\max(\varepsilon_K) = 1$). Finally, the additional capacitive tuning presents little to no advantage when associated with PSSHI.

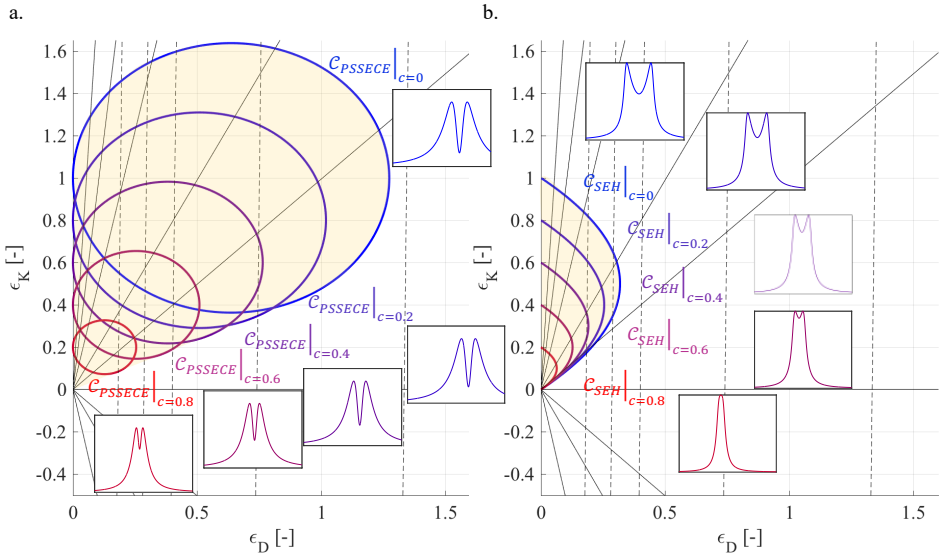

Figure 15. Double-tuning strategies including a combination of single-tuning strategies with an additional capacitive tuning: a. CT-PSSECE and b. CT-SEH.

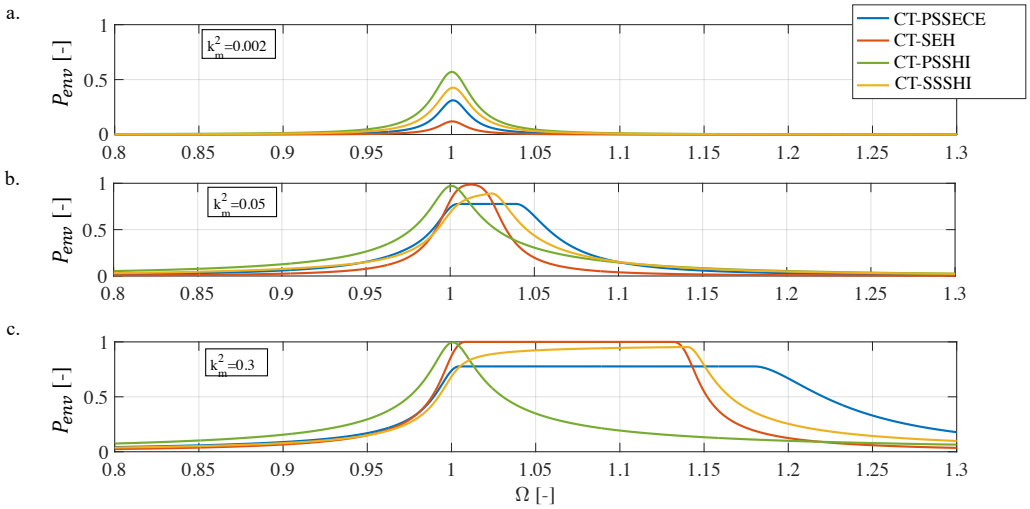

Figure 16. Harvested power envelopes of the CT-PSSECE (blue), CT-SEH (red), CT-SSSHI (yellow), and CT-PSSHI (green), with $Q_m = 50$, $\beta_{min} = -0.8$ and a. $k_m^2 = 0.002$ b. $k_m^2 = 0.05$ c. $k_m^2 = 0.3$

We can observe the directional scaling linked with the additional capacitive tuning. Because of this directional scaling, the resonance frequency tuning range of a capacitively tuned strategy is defined by the maximum value of ε_K — the higher ($\max(\varepsilon_K)$), the larger the harvesting bandwidth of the strategy. In the literature, the PSSECE is the single-tuning strategy that exhibits the highest $\max(\varepsilon_K)=1+2/\pi$, so we can suppose that the PSSECE is the best strategy to combine with capacitive tuning. This prediction is confirmed by the harvested power envelopes of the double-tuning strategies shown in Fig. 16: CT-SEH, CT-PSSECE, CT-SSSHI (SSSHI with an additional capacitive tuning), and CT-PSSHI (PSSHI with an additional capacitive tuning).

Table 4. Table gathering all the analytical expressions of electrical damping and stiffness of well-known CVE (green) and CDE (red) strategies.

	Strategy	Param. $\boldsymbol{\psi_i}$	Dom. $\mathbb{V}_i$	Electrical damping ε_D	Electrical stiffness ε_K	Ref.
No tuning	SECE	-	-	$4/\pi$	1	[10]
	USECE	-	-	$1/2$	$2/\pi$	[53]
Single-tuning strategies ($k=1$)	SEH	$\boldsymbol{r_{dc}}$	$\mathbb{R}^+$	$\frac{8\boldsymbol{r_{dc}}\Omega}{(2\boldsymbol{r_{dc}}\Omega+\pi)^2}$	$\frac{\boldsymbol{r_{dc}}\Omega}{\boldsymbol{r_{dc}}\Omega+\pi/2}$	[33]
	SOR	$\boldsymbol{r_{dc}}$	$\mathbb{R}^+$	$\frac{8\boldsymbol{r_{dc}}\Omega\left[1+\frac{\boldsymbol{r_{dc}}\Omega}{2\pi}\right]}{(\boldsymbol{r_{dc}}\Omega+\pi)^2}$	$\frac{\boldsymbol{r_{dc}}\Omega}{(\boldsymbol{r_{dc}}\Omega+\pi)}$	[38]
	PSSHI	$\boldsymbol{r_{dc}}$	$\mathbb{R}^+$	$\frac{8\boldsymbol{r_{dc}}\Omega\left[1+\frac{\boldsymbol{r_{dc}}\Omega(1-\beta_{\min}^2)}{2\pi}\right]}{[(1-\beta_{min})\boldsymbol{r_{dc}}\Omega+\pi]^2}$	$\frac{1}{1+\frac{\pi}{\boldsymbol{r_{dc}}\Omega(1-\beta_{min})}}$	[34]
	SSSHI	$\boldsymbol{r_{dc}}$	$\mathbb{R}^+$	$\frac{4}{\frac{\pi(1+\beta_{min})}{(1-\beta_{min})}+2\boldsymbol{r_{dc}}\Omega}$	1	[40]
	Mult. SECE	$\boldsymbol{N}$	$\mathbb{N}^*\backslash\{1\}$	$-\boldsymbol{N}\frac{\cos(\pi/\boldsymbol{N})-1}{\pi}$	$1-\frac{\boldsymbol{N}\sin(\pi/\boldsymbol{N})}{2\pi}$	[6]
	Regen. SECE	$\boldsymbol{N}$	$N^{-1}\in\mathbb{N}^*$	$-\frac{2\boldsymbol{N}}{\pi}[(-1)^{1/N}-1]$	1	[6]
	SSECE	$\boldsymbol{\Delta\phi}$	$[0,\pi]$	$\frac{[1+\cos(\boldsymbol{\Delta\phi})]^2}{\pi}$	$\frac{2\pi-2\boldsymbol{\Delta\phi}+\sin(2\boldsymbol{\Delta\phi})}{2\pi}$	[17]
	PSSECE	$\boldsymbol{\phi_s}$	$[-\frac{\pi}{2},\frac{\pi}{2}]$	$\frac{4}{\pi}\cos^2(\boldsymbol{\phi_s})$	$1+\frac{2}{\pi}\sin(2\boldsymbol{\phi_s})$	[16]
	Tun. SECE	$\boldsymbol{\beta_{sw}}$	$[\beta_{min},1]$	$\frac{4}{\pi}\frac{1-\boldsymbol{\beta}}{1+\boldsymbol{\beta}}$	1	[12]
Double-tuning strategies ($k=2$)	SC-SEH	$(\boldsymbol{r_{dc}},\boldsymbol{\Delta\phi})$	$\mathbb{R}^+\times[0,\pi]$	See [35]	See [35]	[35]
	CT-SEH	$(\boldsymbol{r_{dc}},\boldsymbol{c})$	$\mathbb{R}^+\times[0,1]$	$\frac{8\boldsymbol{r_{dc}}\Omega(1-\boldsymbol{c})}{(2\boldsymbol{r_{dc}}\Omega+\pi)^2}$	$\frac{\boldsymbol{r_{dc}}\Omega(1-\boldsymbol{c})}{\boldsymbol{r_{dc}}\Omega+\pi/2}$	[28]
	PS-SSHI	$(\boldsymbol{r_{dc}},\boldsymbol{\phi_s})$	$\mathbb{R}^+\times[0,\pi]$	See [20]	See [20]	[20]
	SCSECE	$(\boldsymbol{\phi_s},\boldsymbol{\Delta\phi})$	$[0,\pi]\times[0,\pi]$	$\frac{[\cos(\boldsymbol{\phi_s})+\cos(\boldsymbol{\phi_s}+\boldsymbol{\Delta\phi})]^2}{\pi}+\sin\frac{(2\boldsymbol{\phi_s})}{2\pi}+2\frac{\cos(\boldsymbol{\phi_s}+\boldsymbol{\Delta\phi})\sin(\boldsymbol{\phi_s})}{\pi}$	$1-\frac{\boldsymbol{\Delta\phi}}{\pi}+\frac{\sin(2\boldsymbol{\phi_s}+2\boldsymbol{\Delta\phi})}{2\pi}$	[19]
	FTSECE	$(\boldsymbol{\beta_{sw}},\boldsymbol{\phi_s})$	$[-\frac{\pi}{2},\frac{\pi}{2}]\times[\beta_{min},1]$	$\frac{4}{\pi}\frac{1-\boldsymbol{\beta_{sw}}}{1+\boldsymbol{\beta_{sw}}}\cos^2(\boldsymbol{\phi_s})$	$1+\frac{2}{\pi}\frac{1-\boldsymbol{\beta_{sw}}}{1+\boldsymbol{\beta_{sw}}}\sin(2\boldsymbol{\phi_s})$	[18]
	TH-SSHI	$(\boldsymbol{r_{dc}},\boldsymbol{\beta})$	$\mathbb{R}^+\times[\beta_{min},1]$	See [22]	See [22]	[22]
	CT-Strat	$(\boldsymbol{\psi_1},\boldsymbol{c})$	$\mathbb{V}_1\times[0,1]$	$(1-\boldsymbol{c})\,\varepsilon_D\vert_{strat}(\boldsymbol{\psi_1})$	$(1-\boldsymbol{c})\,\varepsilon_K\vert_{strat}(\boldsymbol{\psi_1})$	Appendix D